Osaka University Knowledge Archive

Title	X?ray Structure Analysis of Bovine Heart Mitochondorial Cytochrome bc1 Complex
Author(s)	Kawamoto, Masahide
Citation	大阪大学, 1996, 博士論文
Version Type	VoR
URL	https://doi.org/10.11501/3109894
rights	
Note	

Osaka University Knowledge Archive : OUKA

https://ir.library.osaka-u.ac.jp/

Osaka University

X-ray Structure Analysis of Bovine Heart Mitochondorial Cytochrome bc_1 Complex

A Doctral Thesis
by
MASAHIDE KAWAMOTO

submitted to the Faculty of Science, Osaka University

February, 1996

①

X-ray Structure Analysis of Bovine Heart Mitochondorial Cytochrome bc1 Complex

A Doctral Thesis
by
MASAHIDE KAWAMOTO

submitted to the Faculty of Science, Osaka University

February, 1996

Chapter 1
General Introduction 1
1.1. Characteristics of Cytochrome bc_1 Complex 1
1.2. Structural Analysis of Cytochrome bc_1 Complex 2
1.3. Crystallization of Cytochrome bc_1 complex 4

Chapter-2.
Crystallization and Preliminary X-ray Diffraction Studies 8
2.1. Introduction

2.2. Experimental & Results 9
2.2.1. Chemical 9
2.2.2. Purification of Cytochrome bc_1 Complex 9
2.2.3. Crystallization of Cytochrome bc_1 Complex 10
2.2.4. Servey of the Additives 11
2.2.5. X-ray Diffraction Experiment 12

2.3. Discussion 13
2.3.1. The Roles of Zn Cation
2.3.2. Isomorphous Differences
among Different Purified Crystals 14
2.3.3. Difference of Diffraction Intensities
between Crystals with and without $ZnCl_2$ 14

Chapter-3.
X-ray Crystallographic Analysis of Cytochrome bc_1 Complex 20
3.1. Introduction 20

3.2. Experimental 21
3.2.1. Preparation of heavy-atom Derivative 21
3.2.2. Intensity Measurement 22
3.2.3. Processing of Intensity Data 22
3.2.4. Structural Analysis 23

3.3. Results & Discussion 25
3.3.1. Preparation of heavy-atom Derivative Crystlas 25
3.3.2. Crystals Treated with PDTA 26
3.3.3. Determination of Heavy-atom Binding Sites 29
3.3.4. Phase Calculation
by Multiple Isomorphous Replacement 32
3.3.5. Phase Improvement by Density Modification 34

Chapter-4.
Three Dimensional Structure of Cytochrome bc_1 Complex 53
4.1. Introduction 53

4.2. Structure of the bc_1 complex determined by X-ray analysis and comparison with model determined by electron microscopic analysis 53

Conclusion 59
Acknowledgement 60
Reference 61

Chapter-1.
General Introduction

1.1. Characteristics of Cytochrome bc_1 Complex

The cytochrome bc_1 complex, an oligomeric membrane protein, is the most common type of pump responsible for transfer of protons across energy-transducing membranes, coupled with electron transfer from quinol to *c* - type cytochrome (Trumpower, 1990). The proton gradient produced by this pump is utilized for ATP synthesis. This enzyme is widely distributed among living organisms from bacteria to mammals. Analogous enzyme, b_6f type, occurs in photosynthetic apparatus, chloroplast and so on (Hauska *et al.*, 1983). They all contain four redox centers, two *b* - type and one *c* - type cytochromes and a Rieske-type iron-sulfur center. However, the number of subunits is diverse; ranging from three in the *Paracoccus denitrificans* enzyme (Yang & Trumpower, 1986) to 11 in the mammalian one (Weiss, 1987).

Mitochondrial cytochrome bc_1 complex (E.C. 1.10.2.2) is an integral membrane protein located in the inner membrane, which catalyzes the electron transfer from ubiquinol to cytochrome *c* coupling with proton translocation across the membrane (Hatefi, 1985). This enzyme constructs the energy coupling site II in respiratory chain. In 1960's, the enzyme was isolated from beef heart by Hatefi *et al.* (1962) for the first time. The improvement of purification of the enzyme has enabled to identify the enzyme compositions: molecular weight of a functional unit was estimated to be ca. 250k by fluid physical techniques (Tzagoloff *et al.*, 1965; Weiss & Kolb;, 1979). The unit consists of 11 different polypeptides (Weiss, 1987), in which 2 protohemes, 1 heme *C* and 1 [2Fe-2S] iron-sulfur cluster were contained as prosthetic groups (Rieske, 1976). By determination of the amino acid sequences of subunits I and II by cDNA technique (Gencic *et al.*, 1991), the primary structures of all subunits have been completed (Anderson *et al.*, 1982; Wakabayashi *et al.*, 1982a; 1982b; 1985; Schägger & von Jagow, 1983; Borchart *et al.*, 1985; 1986; Schägger *et*

al., 1985; 1987). The molecular weight of the functional unit estimated from the amino acid sequences is 230k, assuming that it contains one mol of each subunit. Table 1.I summarizes current knowledge of the molecular mass and the topography of the subunits. The five large subunits are common to the mitochondorial cytochrome bc_1 complexes from various sources. Three of these subunits, i.e., cytochrome *b*, cytochrome c_1, and the Rieske iron-sulfur protein, contain redox prosthetic groups and are essential for the enzymatic function. The two largest subunits, core I and core II proteins, are not involved in electron transfer but are hypothesized to be "relics of an ancient processing peptidase". For three of the six small subunits of the bovine enzyme, functional implication has been suggested; subunit VII is identified as a quinone-binding protein; subunit VIII may facilitate the binding of cytochrome *c* to cytochrome c_1; subunit IX may be involved in proton translocation. The roles of subunits VI, X, and XI remain to be explored.

The redox behavior of the purified enzyme, as well as membrane bound form, has been studied most extensively using various inhibitors (Hatefi, 1985). The results obtained, especially the oxidant-induced reduction of cytochrome *b* in the presence of antimycin A (Rieske, 1971), strongly suggest a cyclic electron transfer reaction within the enzyme molecule. Several mechanisms have been proposed for the electron transfer within the molecule, coupled with proton translocation (Croft *et al.*, 1983; de Vries, 1986; Wikström & Krab, 1986). Here, the Q-cycle mechanism (Mitchell, 1976) is presented as one of these working hypotheses (Fig. 1.1).

1.2. Structural Analysis of Cytochrome bc_1 Complex

In spite of extensive functional studies, reaction mechanism of the enzyme has not been understood due to lack of detailed three-dimensional structure. Structural information about cytochrome bc_1 complex is very limited at present.

Subunit proteolysis and labeling with hydrolhilic reagents have revealed which

subunits are exposed to the surface on each side (Gonzalez-Halphen *et al.*, 1988; D'Souza & Wilson, 1982; Bell *et al.*, 1979). Interpretaion of hydropathy plots from a number of species has led to a model for the cytochrome *b* of eight or nine transmembrane helices, with the two heme groups suspended between four histidines on two helices (Widger *et al.*, 1984; Sarraste, 1984; Crofts *et al.*, 1988). Cytochrome c_1, the iron-sulfer protein, and the smaller subunits each contain a single predicted hydrophobic or amphipathic helix that could serve as a membrane anchor (Link *et al.*, 1986). Cytochrome c_1 can be prepared as a water-soluble protein from *Neurospora crassa* by a single proteolytic cleavage that removes the hydrophobic C-terminal domain (Li *et al.*, 1981a). The core I and core II proteins are on the matrix side, and can be isolated from the *N. crassa* enzyme as a water-soluble dimer (Li *et al.*, 1981b).

The structural analysis of this enzyme with electron microscopy had been individually carried out by 2 groups. Leonard and his co-workers obtained the three-dimensional structure of the *Neurospora* bc_1 complex and its subcomplex lacking the two core proteins and the Rieske protein from two-dimensinal crystal (Leonard *et al.*, 1981; Karlsson *et al.*, 1983). Although the resolution is limited (25 Å in the direction parallel to the membrane and 35 Å in the normal direction), these results have provided current basis for considering the arrangement of the subunits; the complex is dimeric; it is elongated across the membrane projecting ~70Å into the matrix of mitochondoria and ~30Å into the intermembrane space; the monomers contact each other in the membrane and in the matrix space. Akiba and his co-workers crystallized the bovine heart mitochondorial bc_1 complex in tubular form and revealed its three-dimensinal structure at 13 Å resolution by helical image reconstruction (in preparation). This result showed not only the elongated shape and the dimeric form of the molecule observed by Leonard *et al.*, but also more detailed structures; narrow transmembrane segments and extensive density along the surface of the membrane.

1.3. Crystallization of Cytochrome bc_1 complex

In order to determine the structure of this enzyme at higher resolution by the X-ray crystallographic analysis, crystallization had been attempted by several groups. Ozawa *et al.* reported needle-shaped microcrystals obtained by dialysing away detergent from solubilized preparations. Gros *et al.* grew needle-shaped crystals up to 0.7 mm in length by vapor diffusion. Recently, Yue *et al.* have crystallized bovine heart mitochondorial cytochrome bc_1 complex in square or octagonal plates as large as 4 x 2 x 1 mm. None of these groups reported X-ray diffraction. The crystal of this enzyme capable of giving X-ray diffraction spots was obtained by Kubota *et al.* at first in 1991. In the following year, two other groups independently developed crystallization protocols of the cytochrome bc_1 complex from bovine heart mitochondoria (Berry *et al.*, 1992; Yu & Yu, 1993). The crystal giving the highest ability to diffract X-ray showed the diffraction spots to 3.3Å resolution. As is often found for other large proteins, these crystals diminish the capability of X-ray diffraction by exposing to X-ray, thereby posing a difficult obstacle in obtaining a complete data set. Because the crystals of this enzyme lack isomorphism to each other as often observed for other complex crystals, merging and scaling of the data sets obtained from different crystals are impossible. This situation also makes preparation of useful isomorphous heavy-atom derivative crystals difficult, and hampers successful determination of the three-dimensinal structure of this enzyme.

Although the crystals of cytochrome bc_1 complex were obtained, there were problems in reproducibility and quality of the crystals as well as in methodology of X-ray analysis for such large membrane complex crystals. Aiming at the final goal of elucidating functional mechanism of this emzyme, I tried to determine its detailed three dimensional structure. In Chapter-2 is described how I improved the quality of the crytal and overcome a problem of reproducibility of the crystallization. In Chapter-3, preparation of two heavy-

atom derivative crystals and collection of the native and two heavy-atom derivativse using synchrotron radiation are described. Determination of three dimensional structure of cytochrome bc_1 complex at 8 Å resolution is also described in this chapter. Chapter-4 deals with the comparison between the structure determined by X-ray crystallography and that determined by electron microscopy.

Table 1.I. Subunits of the Bovine Cytochrome bc_1 Complex

Subunit	Common name	Molecular weight[1] (Da)	Proposed location in the complex[2]
I	core I protein	49236	matirx
II	core II protein	46530	matrix
III	cycochrome *b*	42590	trnsmembrane
IV	cytochrome c_1	27906	intermembrane space
V	Rieske iron-sulfer protein	21669/21609	intermembrane space
VI	ubiquinone binding protein (?)[3]	13389	matrix
VII	ubiquinonebinding protein	9587	transmembrane[4]
VIII	hinge protein	9172	intermembrane space
IX	DCCD binding protein	7997	intermembrane space
X	—	7298/7326	intermembrane space
XI	—	6520	transmembrane[4]

1) According to the recent results by electron ionization mass spectrometry (Musatov, 1994) except for subunit III, whose molecular weight is calculated from the DNA sequence (Anderson, 1982).

2) According to figure 12 in González-Halphen *et al.* (1988).

3) At present this function is doutful (Usui *et al.*, 1991).

4) No evidence is given for the transmembrane topology (González-Halphen *et al.* 1988).

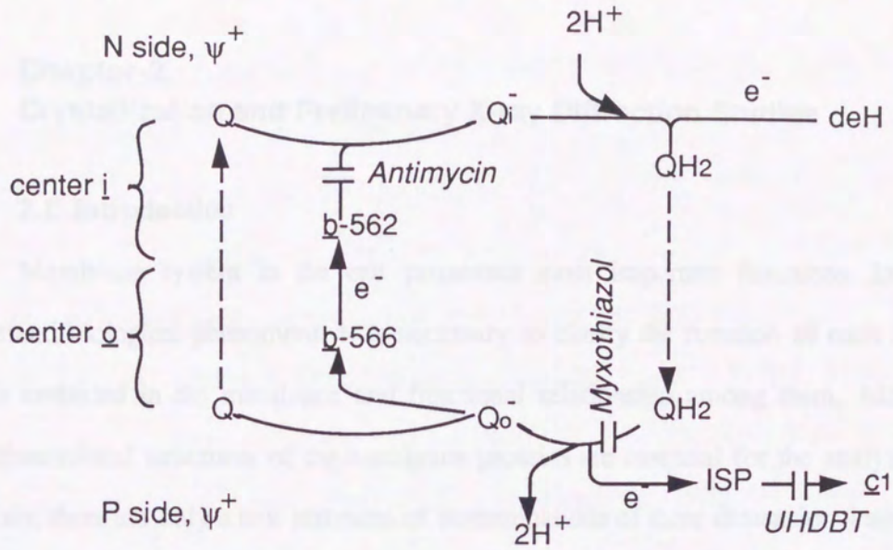

Fig. 1.1. The proposed protonmotive Q-cycle of cytochrome bc_1 complex. The dashed arrows designate specific species of ubisemiquinone anion, which react at the electronegative N (matirx) side (center i) or electropositive P (cytosolic) side (center o) of the inner mitochondorial membrane. ISP, iron-sulfer protein; deH, dehydrogenase. This figure is from (Hatefi, 1985).

Chapter-2.
Crystallization and Preliminary X-ray Diffraction Studies

2.1. Introduction

Membrane system in the cell possesses most important functions. In order to understand biological phenomena, it is necessary to clarify the function of each membrane protein embeded in the membrane and functional relationship among them. Although the three dimensional structures of the membrane proteins are essential for the analysis of thier functions, there are only a few instances of determinations of three dimensional structures of membrane proteins at atomic resolution (Kühlbrandt, 1988; Weiss *et al.*, 1990; Deisenhofer & Michel, 1989). The reason is difficulty of crystallization of membrane proteins purified in detergent-protein mixed micelle, that is entirely different from soluble globular proteins with respect to the chemical behavior. Crystallization is, however, unavoidable process for application of X-ray crystallography, which is the most powerful technique for determination of the three-dimensional structure of whole protein at atomic resolution. Therefore, the crystallization of membrane proteins has been one of the most important and challenging subjects for elucidation of their functional mechanism.

After crystallization of bovine heart mitochondorial cytochrome bc_1 complex was achieved (Ozawa *et al.*, 1980; Gros *et al.*, 1988; Yue *et al.*, 1991), extensive trials improving crystal quality led to produce the crystals giving X-ray diffraction spots by three groups independently (Kubota *et al.*, 1991; Berry *et al.*, 1992; Yu & Yu 1993). In my previous study of crystallization of this enzyme (Kawamoto, 1993), two different crystal forms were obtained; monoclinic crystals grown in Tris-HCl buffer, whose space group and cell dimensions were $P2_1$ and a = 196 Å, b = 179 Å, c = 253 Å, β = 97° (Kubota *et al.*, 1991), and hexagonal one grown in potassium phosphate buffer, whose space group and cell dimensions were $P6_1$ or $P6_5$ and $a = b$ = 131 Å, c = 727 Å (Kawamoto, 1993; Kubota 1993). The monoclinic crystals had several problems for X-ray crystallograhic analysis.

They tended to be twinned and were extremely fragile and diffraction was limited to 7.5 Å resolution. The hexagonal crytals were more stable to mechanic shock, change of circumstance and X-ray irradiation than monoclinic one, and X-ray diffraction ability was also extended to 6.5 Å resolution. There were, however, problems with reproducibility and quality; X-ray diffraction ability of the crystal depended on the enzyme preparation (Kubota, 1993), and crystals prepared from different purification lots lacked isomorphism (Kawamoto, 1993). In order to improve reproducibility and quality of the hexagonal crystals of this enzyme, I examined further crystallization condition of the hexagonal crystal form.

2.2. Experimental & Results

2.2.1. Chemical

Sodium deoxycholate was a product of Nacalai Tesque. Cholate was a reagent of Sigma Chemicals Co. Sucrosemonolaurate (> 99% monoester pure) was a product of MITSUBISHI-KASEI FOOD Co. Ltd. Polyethyleneglycol 4000 (PEG 4000) used for enzyme purification was a Extra Pure Reagents of Wako Co.Ltd. PEG 4000 used as presipitant of crystallization was a reagent of MERK Co. Ltd. for gas chromatography. Other reagents were of the highest grade commercially available.

2.2.2. Purification of Cytochrome bc_1 Complex

The cytochrome bc_1 compex was prepared from fresh bovine heart muscle by the method of Rieske (1967) with slight modifications (Kubota *et al.*, 1992). The purification protocol was described briefly as following. A Keilin-Hartree preparation (Yoshikawa *et al.*, 1977), starting material, was made up from fresh bovine heart within four hours after slaughter. The Keilin-Hartree preparation was suspended into 50 mM Tris-HCl (pH 8.0), 0.66 M sucrose (called 'bufferd sucrose') to 35 mg protein/ml. Extraction of membrane protein was carried out with sodium deoxycholate and potassium chloride. The fraction that

contained succinate-cytochrome *c* reductase was fractionated with ammonium acetate in the presence of deoxycholate. Detergent of the fraction was exchanged to cholate and following fractionation with ammonium sulfate was followed in order to remove succinate dehydrogenase. The detergent, cholate, of final fraction was exchanged for sucrose monolaurate by precipitation with polyethylene glycol 4000 (PEG 4000) in the presence of the latter detergent. Finally the Tris-HCl buffer in the preparation was replaced with potassium phosphate by dialysis. The yield of the final enzyme was 300 - 600 mg from 800 g of minced bovine heart. The preparation contained all of the 11 subunits (data not shown) and had the same absorption spectrum (Fig. 2.1) as that of the authentic sample (Kubota *et al.*, 1991).

2.2.3. Crystallization of Cytochrome bc_1 Complex

Crystallization of this enzyme was performed by the batch method as described previously (Kubota, 1993; Kawamoto, 1993). The crystallization solution contined 40 to 80 mg protein/ml, 0.66 M sucrose, 0.5% (w/v) sucrose monolaurate and 30 to 50 mM potassium phosphate (pH 8.0). Solid PEG 4000 was added until the solution became slightly turbid, after which it was stored at 20 °C. Amorphous material appeared in the super saturated solution one to two days after the addition of PEG 4000, and 1-2 weeks later red crystals of hexagonal columnar form grew in it (Fig. 2.2).

These crystals were large enough (approximately 0.3 x 0.3 x 1.0 mm) for X-ray crystallographic analysis, and more stable to X-ray and mechanical shock than the previous monoclinic one (Kubota *et al.*, 1991). A preliminary X-ray diffraction experiment showed that the crystal system was hexagonal, space group $P6_1$ or $P6_5$ with unit-cell constants of $a = b = 131$ Å and $c = 720$ Å. The V_m value was calculated to be 3.9 Å^3/Da assuming that one dimer was present in an asymmetric unit. This crystal form diffracted X-rays up to 6.5 Å resoluiton.

There was, however, a serious problem of reproduciblity in crystallization. The quality of the crystal depended on the enzyme praparation. For example, only polycrystals were formed, or the crystals obtained did not diffract X-ray or diffraction was limited to very low resolution. Investigatation of the crystallization condition of this enzyme showed that the formation of hexagonal crystals depended critically on the concentration of the phosphate buffer, and that there is optimum concentration where large and well-orderd crystals were deposited (kubota, 1993). However, the optimum concentration is different from preparation to preparation and the crystals applicable for X-ray crystallographic analysis were seldom obtained.

2.2.4. Servey of the Additives

It is known that such additives as specific inhibitor, substrate and metal salt are required or effective for crystallization. The effect of specific inhibitors and substrate of cytochrome bc_1 complex on its crystallization was investigated to show that neither the inhibitors (antimycin A and myxothiazol) nor substrate (horse heart cytochrome *c*) were effective for crystallization (Kubota, 1993). Then, I tested the effect of metal salts, particularly divalent cations, on crystallization of this enzyme, because Lorusso *et al.* (1991) reported that zinc cation inhibited this enzymatic reaction.

Each divalent metal salt ($MgCl_2$, $CaCl_2$, $ZnCl_2$, $CdCl_2$ and $HgCl_2$) used was dissolved in distilled water at 200 mM then added to the enzyme solution at 1 to 10 mM prior to the addition of PEG 4000. All of the additives tested decreased the enzyme solubility. $HgCl_2$, especialy, caused the immediate aggregation of the enzyme. No apparent effect on the crystallization and crystal growth of this enzyme was observed by the addition of divalent metal salt except $ZnCl_2$. $ZnCl_2$ had a marked effect on crystallization. Addition of 1 to 4 mM $ZnCl_2$ to the enzyme solution resulted in a decrease in enzyme solubility, numerous hexagonal microcrystals appearing immediately at PEG 4000 consentration of 2 to 4 %

(w/v). The nucleation frequency was higher at a low concentration of potassium phosphate. Crystals with sharp edges grew large enough for X-ray crystallographic analysis when the nucleation frequency was moderate (Fig. 2.3). An addition of $ZnCl_2$ significantly improved the reproducibility of the crystallization and the quality of the crystals. Single crystals were obtained in the presence of $ZnCl_2$ from almost all the enzyme preparation examined, even from the one that yielded only polycrystals when $ZnCl_2$ was omitted. Moreover, the crystals obtained had better shape and increased clarity. When zinc acetate or zinc sulfate was added into the enzyme solution in order to examine the effect of counter anion, crystal growth was also improved as observed when $ZnCl_2$ was added. Thus, this effect on crystallization seems to be due to zinc cation. In the case that $ZnCl_2$ was absent from crystallization solution, the nucleation frequency and the shape of the crystals was depended on the concentration of the enzyme and phosphate buffer (Kubota, 1993). Therefore, their optimum concentrations had to be examined in every purification lot of this enzyme. By the addition of $ZnCl_2$ to crystallization solution, the optimum concentration of enzyme and buffer were nearly constant against any purification lots. Standard conditions of crystallization of this enzyme in the presence of $ZnCl_2$ were summarized in Table 2.I.

2.2.5. X-ray Diffraction Experiment

X-ray diffraction experiments were done using a screenless Weissenberg camera for macromolecular crystals (Sakabe, 1991) and synchrotron radiation at the BL6A beamline of the Photon Factory, the National laboratory for High Energy Physics, Tsukuba, Japan. The SR-ray was focused by a cylindrical-bent asymmetric cut Si(111) monochromator. The temperature was kept at 20 ℃ throughout the experiment. The X-ray wavelength used was 1.000 Å, and the collimator size was 0.1 mm. The cassette, which attached a 200 x 400 mm imaging plate (Fuji Photo Film Co. Ltd), had a radius of 859.5 mm. Each crystal was sealed in a quartz capillary just before the diffraction experiment. After several exposures the crystal

was translated to avoid deterioration of the diffraction pattern. In this manner, each data set was obtained with one crystal. The diffraction pattern recorded on the imaging plates were digitized at 100 μm intervals on a Fujix BA-100 read-out system. The intensity data on the imaging plates were processed with the program *WEIS* (Higashi, 1989) then merged and scaled with the program *PROTEIN* (Steigemann, 1974).

The crystals obtained in the presence of $ZnCl_2$ diffracted X-ray to 6.5 Å resolution as well as one obtained in the absence of $ZnCl_2$ (Fig. 2.4). Although the cell dimensions along the *a* and *b* axes as well as the space group were unchanged by the addition of $ZnCl_2$, the dimension along the *c* axis increased slightly (~0.5 %). Since the diffractions were often limited to rather low resolution, the estimates of the cell dimension of the crystals were not so accurate that correlation between the dimension of *c* and the presence of $ZnCl_2$ was unclear. The result of intensity measurements for both the crystals are given in Talbe 2.II, and the completeness and R_{merge} *versus* resolution are given in Table 2.III. From these results it is clear that the addition of $ZnCl_2$ improved the diffraction quality of the crystal as well as the reproducibility of crystallization.

2.3. Discussion

2.3.1. The Roles of Zn Cation

The reproducibility of crystallization and the quality of the crystal were improved by the addition of $ZnCl_2$ in the crystalliation solution. What is the role of zinc cation in crystallization? It is assumed that zinc cation is bound to the cytochrome bc_1 complex. zinc cation react with phosphate present in phosphate buffer to form zinc phosphate, which is insoluble in water. Although the crystallization solution was buffered by potassium phosphate, no precipitation was appeared when the $ZnCl_2$ was added. Lorusso *et al.* studied the interaction of zinc cation with the cytochrome bc_1 complex and showed that zinc cation

was bound to the hydrophilic subunits and inhibited the reaction of the enzyme (Lorusso *et al.*, 1991).

It is speculated that zinc cation enlarge the specific interaction of the enzyme. Addition of zinc cation decreased the enzyme solubility, and caused the change of cell dimension along only the *c* axis. zinc cation is also essential to the tubular crystallization of cytochrome bc_1 complex (Akiba *et al.*, in preparation). Since the solution for crystallization in tubular form yielded only proteoliposomes if $ZnCl_2$ was absent, it is assumed that zinc cation enables the specific and suitable inter-molecular contacts.

2.3.2. Isomorphous Differences among Different Purified Crystals

Several data sets from crystals grown in the presence of $ZnCl_2$ have been collected. The R_{merge} (in *I*) of each data sets were 9 to 11 %, and the isomorphous differences were about 10 % (in *F*). In my previous studies of crystallization of cytochorme bc_1 complex (Kawamoto, 1993), the R_{merge} of data sets collected from crystals grown in the absent of $ZnCl_2$ were 10 to 14 % (in *I*) and the isomorphous differences were 15 to 20 % (in *F*). It may be concluded from these results that the addition of $ZnCl_2$ decreased the isomorphous differences among the purification lots. Nevertheless, the isomorphous difference appears still too high to permit merging the data sets from crystals of the different purification lots.

2.3.3. Difference of Diffraction Intensities between Crystals with and without $ZnCl_2$

Diffraction intensities of the crystals grown in the presence of $ZnCl_2$ differed from those grown in its absence. The isomorphous difference between the data sets listed in Table 2.II was about 16 % (in *F*). Since the data sets compared in Table 2.II were collected from crystals of the different purification lots, so the possibility that the difference of diffraction

intensities was caused by the difference of purification lots, and addition of $ZnCl_2$ can not be ruled out.

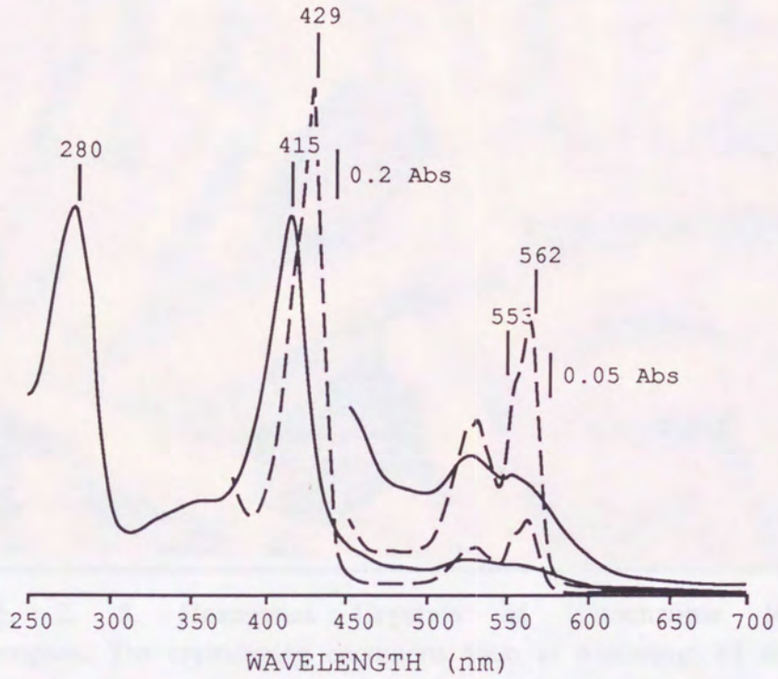

Fig. 2.1. Absorption spectrum of purified cytochrome bc_1 complex. The enzyme was diluted into buffered sucrose (pH 8.0) containing 0.5 % (w/v) sucrose monolaurate. Solid lines represent the purified enzyme and dished lines represent dithionite-reduced form.

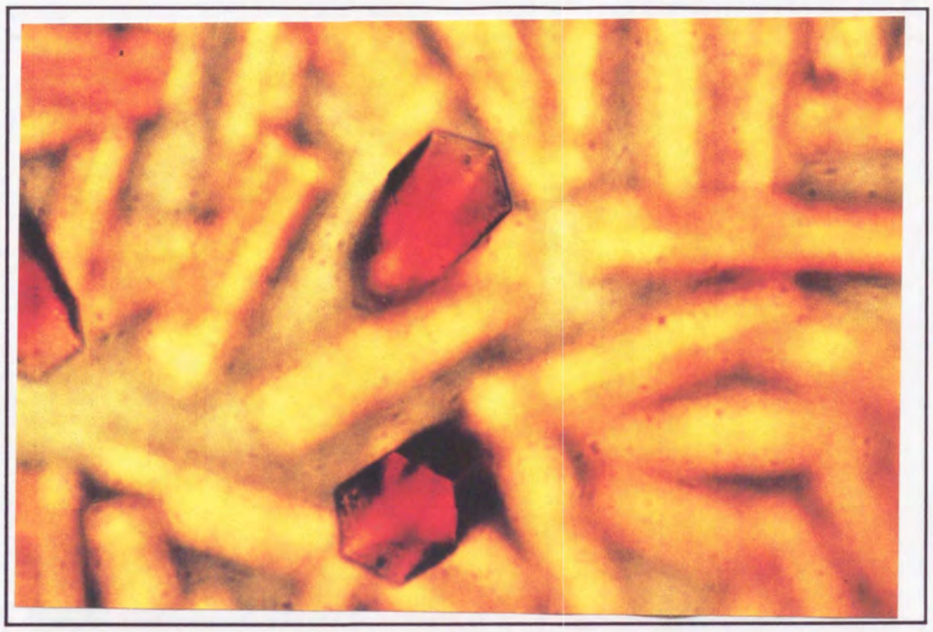

Fig. 2. 2. Hexagonal Crystals of Cytochrome bc_1 Complex. The crystallizing conditions were as following: 88 mg protein/ml, 0.66 M sucrose, 50 mM potassium phosphate (pH 8.0) and 0.5 % (w/v) sucrose monolaurate. PEG 4000 concentration was 8.4 % (w/v). The overall dimension of the area in the photograph is 1.4 x 2.1 mm.

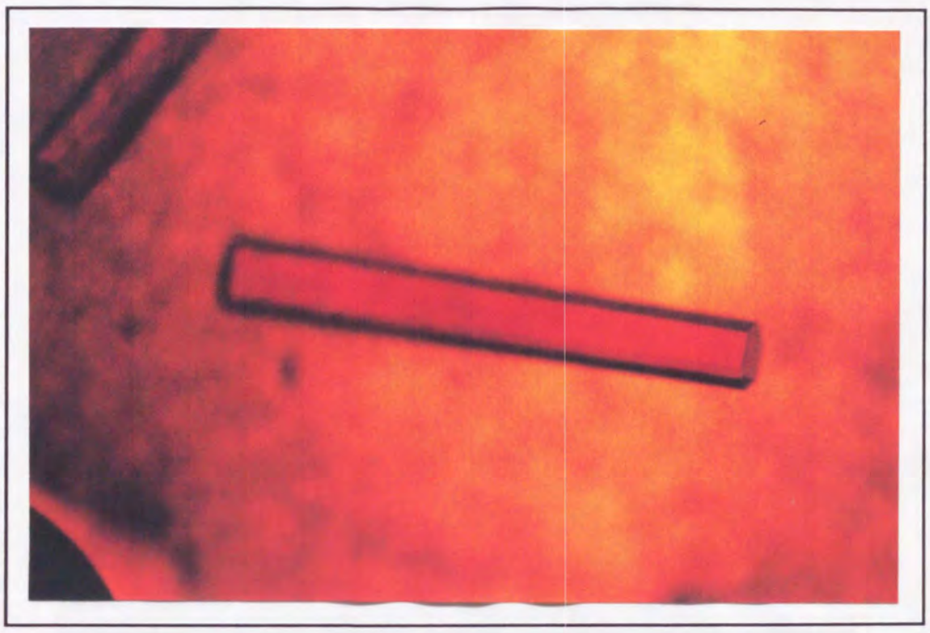

Fig. 2.3. Hexagonal crystals of cytochrome bc_1 complex grown in the presence of $ZnCl_2$. The crystallization conditions were the same to those listed in Table 2.I. PEG 4000 concentration was 6.5 % (w/v). The overall dimension of the area in the hotograph is 1.4 x 2.1 mm.

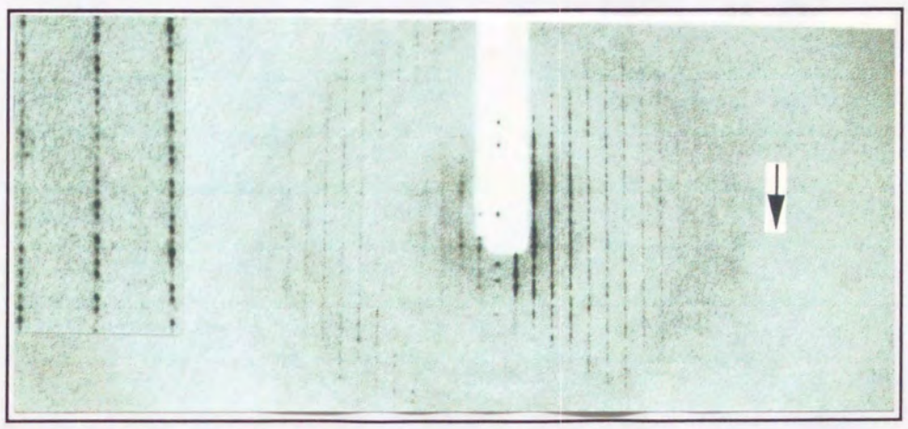

Fig. 2.4. Diffraction Patterns of the Crystal Grown in the Presence of $ZnCl_2$

Arrowhead indicates the 7.0 Å resolution range. Inset is the close-up (x4) of this photo.

Table 2.I. Standard Conditions of Crystallization with $ZnCl_2$

Protein	57.5 mg / ml (250 μM c_1)
Sucrose	0.66 M
Potassium phosphate	40 mM (pH 8.0)
Sucrose monolaurate	0.5 % (w/v)
$ZnCl_2$	4 mM
PEG 4000	5 - 7 % (w/v)

PEG 4000 : polyethylene glycol 4000

Table 2.II. The Conditions and The Results of Intensity Mesurements

	- $ZnCl_2$	+ $ZnCl_2$
Oscillation angle (°)	3.75	5.25
Range of data collection (°)	52.75	60.25
Exposure (s)	75	105
Number of imaging plates	15	12
Resolution range (Å)	30.0 - 8.0	30.0 - 8.0
Mesured reflections ($F > 2\,\sigma_F$)	13,470	18,940
Unique reflections ($F > 2\,\sigma_F$)	5714	6459
Completeness (%)	76.6	88.5
R_{merge} (%)	12.33	10.15

Completeness = (No. of reflections with $F > 2\,\sigma_F$) / (No. of total possible reflections).

$R_{merge} = \Sigma_h \Sigma_i |I_{hi} - \langle I_h \rangle| / \Sigma_h \Sigma_i \langle I_h \rangle$.

Table 2.III. R_{merge} *versus* Resolution Range

Resolution (Å)	Completeness (%)	R_{merge} (%)
– 13.4	98.1	5.9
13.4 – 10.8	96.3	13.2
10.8 – 9.5	93.4	17.1
9.5 – 8.6	85.0	20.3
8.6 – 8.0	71.8	20.4
Total	88.5	10.15

Competeness = (No. of reflections with $F > 2\,\sigma_F$) / (No. of total possible reflections).

$R_{merge} = \Sigma_h \Sigma_i |I_{hi} - \langle I_h \rangle| / \Sigma_h \Sigma_i \langle I_h \rangle$.

Chapter-3.
X-ray Crystallographic Analysis of Cytochrome bc_1 Complex

3.1. Introduction

Structure determination of a protein is a prerequisite to understanding the structure-function relationship. Although the Q-cycle hypothesis is proposed as a reaction mechanism of cytochrome bc_1 complex (Mitchell, 1976), there is no structural basis supporting this hypothesis and many experimental results inconsistent with this hypothesis were reported (Esposti & Lenaz, 1982; De Vries, 1982; Hatefi & Yagi, 1982; Von Jagow *et al.*, 1984; Kauten *et al.*, 1987). The structural information concerning the arrangement of the four redox centers, substrate-binding sites and proton channels urgently needed.

Although X-ray crystallography is the most powerful technique for determination of three-dimensional structure of a protein at atomic resolution. Two major barriers lie for application of this method; preparation of suitable crystals and solution of the phase problem. Although several groups obtained crystals of this enzyme (Kubota *et al.*, 1991; Berry *et al.*, 1992; Yu & Yu 1993), at present none of these determined its three deminsional structure hampered by the phase problem.

In this study, I tried to solve the phase problem by the isomorphous replacement method (Green *et al.*, 1954). Application of this method requires the X-ray diffraction data of the native protein crystal and that of the isomorphous heavy-atom derivative one, the crystal modified by heavy-atom reagents at specific sites of the molecule. When the positions of heavy-atom binding sites in the unit-cell are known, phase angles are calculated on the basis of the difference between the diffraction intensities of the native and derivative crystals. In this chapter, preparation of heavy-atom derivative crystals, determination and refinement of the heavy-atom parameters, and phase improvement by density modification are described.

3.2. Experimental

3.2.1. Preparation of heavy-atom Derivative

Chemical — Phosphotangstic acid (PDTA) was a product of Sigma Chemical Co. Mercury(II) potassium iodide (TIOHG), sodium ethylmercurithiosalicylate (EMTS) and gold(I) potassium cyanide (DCNAU), were purchased from Nacalai Tesque. Tetrakis(acetoxymercuri)methane (TAMM) was a reagent of STREM CHEMICALS. *p*-(Chloromercuri)benzoic acid (PCMB) was a product of Wako Chemical Industries Ltd. Potassium tetracyanoplatinate(II) trihydrate (TCNPT) was purchased from Aldrich Chem. Co. 2,6-Diiodo-4-(2,2-dicyanovinyl)phenol (COMPA) was kindly synthesized by Tokutake (Tokutake, 1992). $(PtC_4O_6N_4H_{10})_2$ (TMPT) and Mo_6Cl_{14} (HMOCL) were kindly supplied by Prof. K. Miyamoto of Kitasato university (Miyamoto, 1994) and Dr. T. Yamagata, Fucalty of Engineering Science of this university. Other reagent were of the highest grade commercially available.

Preparation of heavy-atom derivative crystals — Crystals of heavy-atom derivatives were prepared by the soaking method. The crystals grown in the presence of $ZnCl_2$ were used as the native crystals. They were soaked into each heavy-atom solution. The screening of heavy-atom reagents was carried out under various conditions (see sections 3.2.2. and 3.2.3). The soaking solution was bufferd by 40 mM potassium phosphate and containing 0.66 M sucrose, 0.5 % (w/v) sucrose monolaurate, 15 to 20 % (w/v) PEG 4000, and adequate consentration of heavy-atom regents and additives. Concentration of PEG 4000 used was higher than that of crystallization in order to prevent crystals from dissolving. $ZnCl_2$ was not contained in the soaking solution because of its insolubility in the phosphate buffer. COMPA and HMOCL were dissolved in dimethylsulfoxide (DMSO) at ca. 20 mM then added to the soaking solution. Tetra(acetoximercuri)methane (TAMM) was dissolved in water at ca. 20 mM in the presence of 1 M ammonium sulfate then added to the soaking solution. Other heavy-atom reagents were dissolved in water at more than 10 mM then added

to the soaking solution.

3.2.2. Intensity Measurement

As native crystals from different purification lots were sometimes non-isomorphous (Kawamoto, 1993), data sets of derivative crystals and native one of same purification lot were collected every time.

Intensity measurements of the native and heavy-atom derivative crystals were carried out with synchrotron radiation at the BL6A and BL18B of the Photon Factory, the National Laboratory for High Energy Physics, Tsukuba, Japan. At the both beamlines, the SR-ray was focused by a cylindrical-bent mirror and monochromatiized by a Si(111) monocrhromator. The collimator size was 0.1 mm at BL6A and 0.2 mm at BL18B. A 200 x 400 mm imaging plate was attached to the cassette, which had a radius of 859.5 mm at BL6A and 1290 mm at BL18B. The X-ray wavelength used was 1.000 Å, and the temperature was kept at 20 °C through the experiment at both beamlines. Each crystal was sealed in a quartz capillary just before the diffraction experiment. After several exposure the crystal was translated to avoid deterioration of the diffraction pattern. In this manner, each data set was obtained with one crystal. The diffractions recorded on the imaging plates were digitized at 100 μm intervals on a Fujix BA-100 read-out system and Fujix BAS2000 read-out system.

3.2.3. Processing of Intensity Data

The indexing of diffraction spots and the collection of the integrated intensities were carried out by a program *WEIS* (Higashi, 1989). The intensities collected from different imaging plates were merged and scaled into single data set by a program *PROTEIN* (Steigmann, 1974) in the resolution range from 30.0 Å to 8.0 Å and the structure amplitudes larger than 2 σ level were used. The structure amplitudes of derivative cryatals were scaled to those of native by the Wilson plots, then isomorphous differences were calculated by a program *CMBISO* in program package PHASES (Furey *et al.*, 1990).

to those of native by the Wilson plots, then isomorphous differences were calculated by a program *CMBISO* in program package PHASES (Furey *et al.*, 1990).

3.2.4. Structural Analysis

The structural analysis was performed by a program package *CCP4* (CCP4; SERC Daresbury Laboratory, 1994) and program package *PHASES* (Furey *et al.*, 1990).

Difference Patterson summation — Difference Patterson coefficients $(|F_{PH}| - |F_P|)^2$ between the each derivative and the native were obtained by the program *TOPDEL*, then difference Patterson map was calculated with a program *FSFOUR* .

Refinement of heavy-atom parameters and phase calculation by isomorphous replacement — Isomorphous replacement refinement was carried out by the maximum likelihood method using a program *PHASIT*. Initial occupancy and temperature factor of the heavy-atom were set to 1.0 and 50 Å^2, respectively. The parameters were refined as the following sequence; the relative scaling and temperatue factor of derivative data against to native one, coordinates and occupancy of heavy-atoms and estimation of 'lack of closure' error. The temperature factor of the heavy-atom was fixed to 50 Å^2 throughout the refinement. Phase angles were computed at the last refinement cycle.

Difference Fourier summation — The difference Fourier coefficients (F_{PH} - F_P) and the phase angles were merged by a program *MRGDF*. For self-difference Fourier summation, the structure amplitudes of a derivative utilized in phase calculation were used as F_{PH}, and rescaled to those of the native with relative scaling and temperature factor refined in the heavy-atom parameter refinement. For cross-difference Fourier summation, the structure amplitudes of the other derivative utilized in phase calcuation were used as F_{PH}, but not rescaled to those of native. The difference Fourier map was calculated by a program *FSFOUR*.

Solvent flattening — Solvent flattening was carried out by the means of Wang's

method (Wang, 1985) using a program *BNDRY*. The solvent mask was calculated using a conservative solvent content of 65.5 % (calculated from V_m value (Matthews, 1968) of this crystal) and a 20 Å averaging radius. Using this mask the regions of protein and solvent were determined, and the mean density in the solvent region and the maximum density in the protein region was calculated. $F(000)/V$ was then estimated from these values using following empirical relationship:

$$(|\rho_{solvent}| + F(000)/V) / (\rho_{max} + F(000)/V) = 0.43$$

The density in solvent region was flattened to $(|\rho_{solvent}| + F(000)/V)$. In protein region, the density was set to zero if it was negative and to $(\rho_{max} + F(000) / V)$ if it was positive value. The new phase angles were computed from modified electron density map by a program *MAPINV*, and were combined to original phase angles by using the phase distribution function expressed as Hendrickson-Lattman coefficients.

Searching for non-crystallographic two-fold axis — The electron density map was calculated with the phase angles refined with the solvent flattening procedure by a program *FSFOUR*. A region containing one dimer was extracted by a program *EXTRMAP*. The molecular envelope mask was defined using a program *MAPVIEW*. The extracted region using molecular envelpoe mask was put into P_1 cell which consisted of cell lengths as twice as the size of extracted region. The structure factors of this P_1 cell were calculated by a program *MAPINV*, then self-rotation function was calculated by a program *POLARRFN* using structure factors in resolution range from 100 Å to 14 Å. Other parameters used in this calculation were following; integration radius was 100 Å, averaging radius was 20 Å. The polar angles (ω, φ) obtained were refined by a program *LSQROT* with the electron density map of P_1 cell.

Non-crystallographic symmetry averaging — The electron density map was calculated with multiple isomorphous replacement (MIR) phase angles by a program *FSFOUR*. The molecular envelope mask which covered one dimer was defined from solvent-

calculated with multiple isomorphous replacement (MIR) phase angles by a program *FSFOUR*. The molecular envelope mask which covered one dimer was defined from solvent-flattened MIR map using a program *MAPVIEW*, solvent mask was also obtained from solvent-flattened MIR map using a program *BNDRY*. The MIR map was modified as following; (1) averaging the corresponding electron densities related by the non-crystallographic two-fold axis in the molecular envelope and replacing the density for each molecule with the average by a program *MAPAVG*, (2) leveling the density in the solvent region and truncating the negative density in the protein region using solvent mask by a program *BNDRY*, (3) inverting the modified map to obtain new phase angles by a program *MAPINV*, (4) merging the new phase angles to original MIR phase by a program *BNDRY*, (5) the electron density map was calculated and used in next averaging cycle. These processes were repeated sixteen times. The resulting phase angles were used for the definition of new solvent mask and molecular envelolpe mask. These new masks were applied for the next averaging.

3.3. Results & Discussion

3.3.1. Preparation of heavy-atom Derivative Crystlas

Soaking conditions and diffraction ability — The heavy-atom reagents used and the conditions of soaking are summarized in Table 3.3.I. Crystals were soaked for one to two hours because soaking for more than 6 hours usually caused deterioration of the diffraction patterns. Most derivative crystals diffracted X-ray to as high as the native crystals, but there were only a few derivatives suitable for X-ray analysis. The crystals soaked into 0.5 mM TAMM solution containing 25 mM ammonium sulfate gave limited diffraction. The cell dimensions along the *a* and *b* of derivatives (EMTS, PCMB and HMOCL) soaked under pH 8.0 drastically changed to double of those of the native crystals. The diffraction spots of derivative crystals that prepared with TMPT, TIOHG or TAMM (pH 8.0) streaked and were splitted though crack in these crystals was not observed in microscope. Except for those

derivatives, the diffraction patterns of derivatives were suitable for X-ray analysis. It should be noted that crystals soaked into solution contining PDTA sometimes diffracted X-ray nearly to 4 Å resolution though the native crystals obtained in same purification lot showed the diffraction ability only to about 6 Å resolution.

Data collection — The diffraction intensities of derivatives that prepared with 0.05 mM TAMM (pH 7.2), HMOCL (pH 7.2) or PDTA and those of corresponding native crystals were collected. The experimental conditions and results of data processing for the derivative and the corresponding native crystals were summarized in Table 3.3.II.

The derivative crystals had higher mosaicity than that of the corresponding native crystals, so that quality of derivative data sets was slightly worse than that native sets. The data sets 1 and 2 shown in Table 3.3.II are of sufficient qualities for X-ray crystallographic analysis.

3.3.2. Crystals Treated with PDTA

"PDTA treatment" — The PDTA derivatives had an ability to diffract X-ray to nearly 4 Å resolution, thus it was expected that the diffraction intensities to higher resolution could be collected by a "PDTA treatment". Crystals were treated with PDTA (soaked for 2 hours into solution buffered with 40 mM potassium phosphate at pH 7.2 and containing 0.5 mM PDTA, 0.66 M sucrose, and 0.5 % (w/v) sucrose monolaurate) before the data collection. The crystals soaked into the solution containing PDTA were used as native in crystallographic analysis.

Soaking conditions and diffraction ability — Heavy-atom derivatives were prepared by soaking the PDTA treated crytals into each heavy-atom solution containing 0.5 mM PDTA as additive. When a heavy-atom solution did not contain PDTA, the prepared derivative crystals did not give good diffractions. The soaking conditions are shown in Table 3.3.III. All derivatives had ability to diffract X-ray to more than 8 Å, sometimes to 5 Å, resolution. The TIOHG derivative crystal soaked into solution buffered EPPS was cracked

jugded from its diffraction spots.

Data collection — Three sets of the diffraction intensity of PDTA treated crystals and the additionally soaked ones were collected. The experimental conditions and the data reduction were summarized in Table 3.3.IV.

Each data set was collected with sufficient quality for X-ray analysis to 8 Å resolution. Diffraction intensities collected from the heavy-atom derivatives had same quality as that collected from the PDTA treated crystals. Although all these crystals gave diffractions to higher than 5 Å resolution, the diffraction intensities higher than 8 Å resolution could not be collected accurately. Each crystal treated with PDTA had high mosaicity (ca. 0.5° to 1.0°), so that the estimate of of diffractions were worse in high resolution range. It was found in data set 3 that the crystal decayed during the experiment, and the diffraction intensities were collected from only a part of essential region.

Discussion for soaking condition — Genearlly a crystal grown in phosphate buffer is unfavorable for preparing heavy-atom derivatives because most metal cations are hardly soluble in phosphate buffer. The hexagonal crystals of cytochrome bc_1 complex are grown in the presence of potassium phosphate, so I tried to prepare the derivative crystals by soaking into heavy-atom solution buffered with other buffer. For the preparation of TIOHG derivative, the crystal was soaked into the heavy-atom solution buffered with Tris-HCl. Moreover for the preparation of PDTA-treated TIOHG derivatives, the crystal was treated with PDTA solution buffered with EPPS to remove phosphate in the crystal before soaking into TIOHG solution buffered with EPPS. The diffraction spots of these derivatives streaked or were splitted although the crystals still diffracted X-ray to about 6 Å resolution. The crystal of this enzyme appeared unstable in other buffer than phosphate.

The diffraction spots of derivative crystals soaked under pH 8.0, same pH as in crystallization solution, streaked or splitted. HMOCL derivative soaked under pH 8.0 gave only streaked differaction spots, but that soaked under pH 7.2 was good and their diffraction intensities could be collected with sufficient quality for X-ray analysis.

It is assumed that the change of the charge of surface residues by lowering pH prevented excessive binding of heavy-atom reagents.

All heavy-atom solutions and pre-soaking solutions at low pH did not contain $ZnCl_2$. Table 3.3.V summarized isomorphous differences among the native crystals not treated with PDTA. The isomorphous difference of lot 4 between pH 8.0 and 7.2 was significantly smaller (0.086) than that between different purification lots. The isomorphous difference of Lot 1 (8.0) against Lot 4 (8.0) was 0.070, but that against Lot 4 (7.2) increased to 0.099. This indicates that the change of diffractions on soaking the crystals into Zn-free silution at low pH (7.2) is small. As described earlier, if the enzyme was present in the phosphate buffer no precipitation occured when $ZnCl_2$ was added. This syggests the Zn cation bound to the enzyme does not dissociate by soaking into Zn-free solution (see in 2.3.1). Derivative and native crystals soaked in Zn-free solution in Table 3.3.II diffracted X-ray as much as non-soaked crystals. There was, however, no experimental evidence of the binding of Zn cation to the enzyme.

Effect of PDTA — Crystals treated with PDTA diffracted X-ray to higher resolution, nearly 4 Å, than native crystals obtained in same purification lot. Because PDTA has a property to bind to amino groups in protein non-specifically, it is used as the precipitant of proteins, dyes for negative staining in electron micrscopic analysis. Therefore, it is likely that the PDTA bound to the protein molecules to link them in crystal lattice, and the stability against the change of its circumstance and the ability of X-ray diffraction were improved.

Although the PDTA-treated crystals diffracted X-ray to nearly 5 Å resolution, the diffraction intensities to higher than 8 Å resolution could be collected only from lot 1. Table 3.3.VI shows isomorphous differences among PDTA-treated crystals. As compared with Lot 1 and 4, PDTA-treated crystals lacked isomorphism. That may indicate that binding form of PDTA to the molecule differed from one another.

The statistics of data collected from PDTA-treated crystals were not better than those

of the native crystals obtained in same purification lot (see Table 3.3.II). This indicates that the PDTA did not improve the quality of the crystal except for X-ray diffraction ability.

3.3.3. Determination of Heavy-atom Binding Sites

The coordinates of the heavy-atom binding sites are necessary for application of the isomorphous replacement method. The coordinates are generally deduced from location of peaks in the difference Patterson map (Perutz, 1956), which is expressed as:

$$P(u\ v\ w)=(1\ /\ V)\ \Sigma\ (|F_{PH}|\ -\ |F_P|)^2 \cos(2\ \pi\ (hu + kv + lw))$$

The difference Patterson map has peaks at the end of vector between each heavy-atoms. When the heavy-atoms binds to equivalent sites of different molecules related by a crystallographic symmetry, the end of vectors between them lie in a certain plane, so called 'Harker section'. In the present case of space group $P6_1$ or $P6_5$, there are three Harker sections, w = 1/6, 1/3, and 1/2. The coordinates of the heavy-atoms in unit-cell can be determined from the positions of peaks on Harker sections.

Crystal system of this enzyme is hexagonal and space group is $P6_1$ or $P6_5$. This space group has no symmetry except the direction parallel to the c axis. Therefore, the origin of the unit-cell along c axis is arbitrary. In such case the origin along the c axis is chosen arbitrary and the z coordinates of heavy-atoms are expressed as relative distance from the origin. The relative z coordinates of the heavy-atom sites not related by the crystallographic symmetry can not be determined from the positions of peaks on Harker section; they can be determined by analyging the positions of 'cross-vector' in the difference Patterson map, the vectors from one site to another site in the same molecule. If the phase angles are known, the difference Fourier map with the coefficient (F_{PH} - F_P), where F_{PH} and F_P are the structure factors of the derivative and native crystals, will give peaks at the positions of the heavy-atoms.

I tried to determine the heavy-atom sites by means of difference Patterson method,

searching of cross-vector peaks, and self-difference Fourier method.

Isomorphous difference — R_{deriv} of the data sets were listed in Table 3.3.VII and 3.3.VIII.R_{deriv} of all derivatives not treated with PDTA were higher than 0.1. Though R_{deriv} of PDTA derivative in data set 2 was nearly equal to that of other derivatives in the same data set, PDTA derivative in data set 1 particularly showed high isomprphous difference (R_{deriv} = 0.227). This high R_{deriv} may be due to lack of isomorphism. As compared with derivative without PDTA-treatment, R_{deriv} of all PDTA-treated derivatives, except for COMPA and TAMM, were lower than 0.1.

Interpretation of difference Patterson map — Difference Patterson map for all derivatives were calculated. The maps were noisy and had many peaks probably due to lack of isomorphism and the error in intensity data. Determination of the heavy-atom sites was tried by searching consistent peaks on the three Harker sections of each difference Patterson map. For all of derivatives treated with PDTA, however, no consistent peak on the Harker sections could be found. For the TAMM and HMOCL derivatives not treated with PDTA, there were some consistent peaks on the Harker sections; the TAMM derivative gave three consistent peaks, and the HMOCL derivative gave five consistent peaks. Harker sections (W = 1/6, 1/3 and 1/2) and the positions of the consistent peaks for the TAMM and HMOCL derivative were shown in Fig. 3.3.1, and the coordinates of the heavy-atom sites deduced from the positions of peaks were summarized in Table 3.3.IX. The consistent peaks on the diference Patterson map of HMOCL derivative were weaker and broader than those of TAMM derivative, indicating low occupancy or large size of the former heavy-atom reagent.

Determination of the relative z coordinates of the heavy-atom sites was tried by searching the cross-vectors in the difference Patterson map. The maps of both HMOCL and TAMM derivatives were noisy and many peaks appeared that were consistent with the peaks in Harker sections (Table 3.3.X). Therefore it was impossible to pick up correct sets of the

coordinates of the heavy-atom sites.

Self-difference Fourier calculation for each derivative — Since the z coordinates of the heavy-atom sites could not be determined from difference Patterson map, they were tried to be determine from self-difference Fourier map. Chacking each heavy-atom site using self-difference Fourier that I adopted was as following. The phase angles were calculated from only one heavy atom site by single isomorphous replacement method, and the peaks in the resulting difference Fourier map were searched along the z direction with x and y coordinates being fixed at those of the other heavy-atom of the same derivative.

For TAMM derivative, consistent result was obtained; when the Site 1 ($z = 0$) was used for the phase calculation, the peaks correspondng to the Site 2 was appeared at $z = 0.88$ in the resulting difference Fourier map, and *vice versa*. No confident result, however, was obtained for the Site 3 of TAMM, and for all heavy-atom sites of HMOCL derivatives. The difference Fourier map was calculated by the single isomorphous replacement using both Site 1 and Site 2 of TAMM and the peak corresponding to Site 3 of TAMM was checked (Table 3.3.XIII). Though the accuracy of the phase angles must be improved compared with those calculated with only each one site, the peak at Site 3 still could not be observed in the difference Fourier map.

Discussion — Though the R_{deriv} values of both data sets of PDTA derivatives were large (Table 3.3.VII), the peaks in Harker sections of each difference Patterson map could not be interpreted consistently. This suggests non-specific binding of PDTA to the molecules. This coincides with the property of PDTA that it binds to amino groups in proteins non-specifically. Most PDTA-treated derivatives showed low R_{deriv} and gave no consistent peaks on Harker sections of its difference Patterson map. These indicates that heavy-atom reagent did not bind to the molecules with high occupancy. Although HMOCL derivative not treated with PDTA showed high R_{deriv} and the consistent peaks in its Harker sections, HMOCL derivatives treated with PDTA showed low R_{deriv} and did not give

consistent peaks in its Harker section. It was supposed that PDTA binding to the molecules were obstacles for binding of other heavy-atom reagent. The high R_{deriv} of COMPA and TAMM derivative treated with PDTA were perhaps due to lack of isomorphism.

3.3.4. Phase Calculation by Multiple Isomorphous Replacement

Application of isomorphous replacement for solving phase problem requires the information of the heavy-atoms, so called 'heavy-atom parameters', which consist of their coordinates, occupancies and temperature factors. The coordinates determined by the difference Patterson method and other parameters have to be refined in such a way that $|F_{PH}(obs)|$ and $|F_{PH}(calc)|$ approach each other as close as possible.

In the case of phase determination with multiple isomorphous replacement (Green *et al.*, 1954), the positions of the heavy-atoms in all derivatives should be defined with the respect to a same origin. For the space group of the crystal of this enzyme the origin is arbitrary the along *c* axis, and the *z* coordinates of heavy-atoms cannnot be determined by difference Patterson method. As described in the previous section, the relative *z* coordinates of heavy-atom sites were determined for TAMM derivative by the self-difference Fourier method. Since the phase angles were available with a certain accuracy by the single isomorphous replacement using TAMM derivative, the common origin for both derivatives were defined by cross-difference Fourier method.

Determination of common origin — The cross-difference Fourier map were calculated with the coefficient of $(F_{H\,(HMOCL)} - F_P) \exp(i\alpha_{TAMM})$, where $F_{H\,(HMOCL)}$ and F_P are the structure amplitudes of HMOCL derivative and native, α_{TAMM} is the phase obtained with TAMM derivative. Correspondance of the peaks in the cross-difference Fourier map and the positions of heavy-atoms deduced from difference Patterson map was checked; there were no peaks corresponding to Site 1, 2, 3 and 4 of HMOCL derivative in Table 3.3.XI.

The peak appeared at (0.26, 0.13, 0.21) with height greater than 3 σ level and may be correlated to Site 5 of HMOCL derivative (Fig. 3.3.2).

The cross-difference Fourier map was also calculated with the coefficient of $(F_{H}\text{TAMM} - F_{P}) \exp(i\alpha_{HMOCL})$, where $F_{H}\text{TAMM}$ and F_{P} are the structure amplitudes of TAMM derivative and native, and α_{HMOCL} is the phase angles obtained with the heavy-atom parameters of Site 5 of HMOCL derivative by single isomorphous replacement. This map had two peak located at (0.36, 0.07, -0.21) and (0.50, 0.07, 0.67); the former corresponded to heavy-atom at Site 1 and the latter to Site 2 of TAMM derivative. From these analyses of the heavy-atom sites, the common origin between TAMM and HMOCL derivatives were determined.

Phase calculation with multiple isomorphous replacement — The heavy-atom parameters of Sites 1 and 2 of TAMM derivative and Site 5 of the HMOCL derivative were refined by the multiple isomorphous replacement method. Table 3.3.XIV shows the results of each heavy-atom parameters and the statistics of the phase angles. One minor heavy-atom site of TAMM (Site 3) and two minor sites of HMOCL (Site 2 and 4) were located in the diference Fourier map calculated with phase angles by the multiple isomorphous replacement. These minor sites were included in the subsequent refinement. Addition of the minor sites improved the statistics of the phase angles. The final heavy-atom parameters and statistical data of calculated phase angles are shown in Table 3.3.XV.

The occupancy of Site 3 of TAMM was smaller than those of other sites. This may explain why this site could not be defined in the self-difference Fourier map based on the single isomorphous replacement with Sites 1 and 2 of TAMM derivative. Site 5 of HMOCL derivative had higher occupancy than other sites of HMOCL derivative. This agrees with that only the peaks appeared at this site in the cross-difference Fourier map of HMOCL phased by single isomorphous replacement using TAMM derivative.

Native Fourier summation — The electron density map was calculated with the phase angles obtained by the multiple isomorphous replacement. The map is shown in Fig 3.3.3. Because the accuracy of the phases was poor, the molecular boundary could not be determined from the electron density map. Huge ripples appeared around the heavy-atom sites may be due to ill refinement of the heavy-atom parameters.

3.3.5. Phase Improvement by Density Modification

The electron density map of this crystal calculated with the phase angles obtained by multiple isomorphous replacement (MIR) did not have sufficient quality to determine the packing of the molecules in the rystal lattice, molecular shape and location of the subunits. The quality of electron density map can be improved through the refinement of the phase angles by the method of 'density modification'. This method refines the phase angles on the basis of the protein crystals as:

1. The electron density is always positive anywhere in crystal lattice.

2. The electron density in the regions of protein molecules is relatively higher than that in the regions of solvent in the crystal lattice, and the electron density in the solvent region is constant.

3. When the asymmetric unit of the crystal has a number of same molecules, i.e. dimer or trimer, the electron densities of corresponding positions of each molecule are equal. Because of errors remaining in the data sets used for the phases calculations, these features described above do not practically preserved in the electron density map calculated with phase angles obtained isomorphous replacement. The electron density map modified artificially to be adapted to the features described above is considered to be closer to true than that before modification. The density modification method can improve the phase angles by the combination of the new phase angles calculated ftrom modified electron density map to the original MIR phase angles. The density modification method utilizing features 1. and/or

the original MIR phase angles. The density modification method utilizing features 1. and/or 2. is called 'solvent flattening' (especially, using feature 1. is called 'negative truncation') (Wang, 1985), and using feature 3. is called 'non-crystallographic symmetry averaging' (Bricogne, 1976). The improvement of the phase angles was tried by applying the density modification method.

Solvent flattening — Solvent flattening was applied to improve the accuracy of the phase angles. Firstly solvent mask was computed from electron density map calculated with MIR phases. Using this mask solvent leveling and negative density truncation were performed in eight cycles, at the last cycle the refined phase angles were served to compute new solvent mask. This new solvent mask was used in the subsequent modification in eight cycles. R-value, which is defined by $|\Sigma\, |F(\mathrm{obs})| - |F(\mathrm{calc})|| \,/\, \Sigma\, |F(\mathrm{obs})|$, decreased from 0.453 to 0.276 through these refinement cycles. The electron density map calculated from the refined phase angles was shown in Fig. 3.3.4. The electron density of the solvent flattened map defined the molecular boundry.

Searching for non-crystallographic symmetry axis — Electron microscopic analyses of the cytochrome bc_1 complexes from *N. crassa* (Leonard *et al.*, 1981; Karlsson *et al.*, 1983) and from bovine heart mitochondoria (Akiba *et al.*, in preparation) have established that the complex has a dimeric form. The V_m value (Matthews, 1968) of the present crystal suggests one dimeric complex is present in an asymmetric unit. Generally the orientation of the non-crystallographic axes can be determined by the self-rotation function, but for the hexagonal crystals this method often gives inconect result (Tsukihara, personal communication). Thus the electron densities of a whole complex (one dimer) were put into P_1 cell, and the phase angles were calculated, and then determination of the direction of non-crystallographic two-fold axis was tried by the self-rotation function method (see Experimental).

The result is shown in Fig. 3.3.5. The highest peak on the section of $\kappa = 180°$ was

The result is shown in Fig. 3.3.5. The highest peak on the section of $\kappa = 180°$ was located at ($\omega = 67.5°$, $\varphi = 91.7°$). Using these parameters solvent-flattened MIR map was skewed by a program *SKEW*. It became clear from this skewd map that Site 2 of TAMM and Site 5 of HMOCL were located on the non-crystallograohic two-fold axis. These parameters (ω, φ) were refined to (67.9°, 88.8°) by a program *LSQROT* assuming that non-crystallographic axis passes through the position of Site 2 of TAMM. Correlation coefficient between the electron densities related by the non-crystallographic two-fold axis was 0.241.

Non-crystallographic symmetry averaging and solvent flattening — Determination of the parameters of the non-crystallographic two-fold axis opened the way of phase improvement using non-crytallographic symmetry (NCS) averaging together with solvent flattening. Firstly, the solvent mask was computed from electron density map calculated with MIR phases using a 20 Å averaging radius. The phase improvement by solvent flattening using this solvent mask was carried out in eight cycles. The electron density map was calculated with the resulting phase angles, and then was used for defining a molecular envelope mask. The parameters of NCS two-fold axis, the spherical polar angles (ω, φ) defining direction of its axis and the coordinates (x, y, z) of origin of its axis, were refined by the program *LSQROT*. Negative density truncation and solvent leveling using solvent mask were carried out against the electron density map after NCS averaging. After repetition of these procedures by sixteen cycles, a solvent mask and a molecular envelope mask were defined again from NCS averaged and solvent flattened electrn density map. The parameters of NCS two-fold axis were also refined again. New masks and parameters were used for the next averaging cycles. Table 3.3.XVI summarizes the results of overall averaging cycles. This refinement decreased R-factor from 0.454 to 0.322 and improved the correlation coefficient of the electron densities between molecules related by NCS two-fold axis from 0.160 to 0.708. The parameters of NCS two-fold axis at the last refinement cycle were ($\omega = 67.7°$, $\varphi = 91.4°$) and (134.4, 108.6, 274.5).

67.7°, $\varphi = 91.4°$) and (134.4, 108.6, 274.5).

Table 3.3.I Soaking Conditions of Heavy Atom Derivatives

Reagent	M.W.	Concn. (mM)	Buffer (pH)	Additives	Soaking time (hours)	Diffraction[1]
EMTS	404.8	1	40 mM KPI (8.0)	—	1.5	×
PCMB	357.2	1	40 mM KPi (8.0)	—	2	×
TMPT	816.2	0.5	40 mM KPi (7.0)	—	2	×
TIOHG	822.4	1	5 mM Tris-HCl (7.2)	50 mM A.S.	1	×
TAMM	1050.6	0.5	40 mM KPi (7.2)	25 mM A.S.	1	×
		0.05	40 mM KPi (7.2)	2.5 mM A.S.	2.5	O
HMOCL	1110.0	1	40 mM KPi (7.2)	5 %(v/v) DMSO	2	O
PDTA	3417.2	0.5	40 mM KPi (7.2)	—	2	O

1) ×: not diffracted X-ray to higher than 10 Å, O: diffracted X-ray to higher than 10 Å.
EMTS: ethylmercurithiosalicylate, PCMB: *p*-(chloromercuri)benzoic acid,
TMPT: $(PtC_4O_6N_4H_{10})_2$, TIOHG: mercury(II) potassium iodide,
TAMM: tetrakis(acetoxymercuri)methane, HMOCL: Mo_6Cl_{14} , PDTA: phosphotaugstic acid,
KPi: potassium phosphate, A.S.: ammonium sulfate, DMSO: dimetylsulfoxide

Table 3.3.II Experimental Conditions and Statistics of Native and Heavy-atom Derivatives

	data set 1 (Lot 1)		data set 2 (Lot 4)			
	Native	PDTA	Native	PDTA	TAMM	HMOCL
Oscillation angle (。)	5.25	6.25	4.25	4.25	6.25	6.25
Range of collection (。)	60.25	90.25	60.25	44.25	60.25	60.25
Exposure (s)	105	125	85	85	125	125
No. of IPs	12	15	15	11	10	10
Resolution (Å)	30 - 8	30 - 5	30 - 8	30 - 8	30 - 8	30 - 8
Completeness[1]	0.840	0.662	0.890	0.667	0.798	0.822
Multiplicity[2]	2.96	3.13	3.06	2.75	3.00	3.07
R_{merge}[3]	0.120	0.131	0.090	0.077	0.110	0.107

PDTA: phosphotaugstic acid, TAMM: tetrakis(acetoxymercuri)methane, HMOCL: Mo_6Cl_{14}.

1) Completeness = (No. of unique reflections with $F > 2\sigma_F$) / (No. of total possible reflections).

2) Multiplicity = (No. of observed reflections) / (No. of unique reflections).

3) $R_{merge} = \Sigma_h \Sigma_i \, |I_{hi} - \langle I_h \rangle| / \Sigma_h \Sigma_i \, \langle I_h \rangle$.

Table 3.3.III Soaking Conditions of Heavy Atom Derivatives

Reagent	M.W.	Concn. (mM)	Buffer (pH)	Additives	Soaking time (hours)	Diffraction[1]
DCNAU	288.1	1	40 mM KPi (7.2)	0.5 mM PDTA	2	O
COMPA	421.8	1	40 mM KPi (7.2)	0.5 mM PDTA + 5 %(v/v) DMSO	2	O
TCNPT	431.4	1	40 mM KPi (7.2)	0.5 mM PDTA	2.5	O
TIOHG	822.4	1	40 mM KPi (7.2)	0.5 mM PDTA	2	O
			50 mM EPPS (7.2)	0.5 mM PDTA	2	×
TAMM	1050.6	0.05	40 mM KPi (7.2)	0.5 mM PDTA + 2.5 mM A.S.	2	O
HMOCL	1110	1	40 mM KPi (7.2)	0.5 mM PDTA + 5 %(v/v) DMSO	2	O

1) ×: not diffracted X-ray to higher than 10 Å, O: diffracted X-ray to higher than 10 Å.
DCNAU: gold(I) potassium cyanide, COMPA: 2,6-diiodo-4-(2,2-dicyanovinyl)phenol, TCNPT: potassium tetracyanoplatinate(II) trihydrate, TIOHG: mercury(II) potassium iodide, TAMM: tetrakis(acetoxymercuri)methane, HMOCL: Mo_6Cl_{14} , KPi: potassium pjosphate, EPPS: N-2-hydroxyethylpiperazine-N'-3-propanesulfonic acid, PDTA:phosphotaugstic acid, DMSO: dimetylsulfoxide.

Table 3.3.IV Experimental Conditions and Statistics of Native and Heavy Atom Derivatives Treated with PDTA

	data set 1 (Lot 2)			data set 2 (Lot 3)				data set 3 (Lot 4)		
	Native	TCNPT	DCNAU	Native	TCNPT	TIOHG	COMPA	Native	HMOCL	TAMM
Oscillation angle (°)	5.25	5.25	5.25	4.25	4.25	4.25	4.25	4.25	4.25	6.25
Range of collection (°)	60.25	60.25	65.25	60.25	60.25	60.25	60.25	44.25	32.25	30.25
Exposure (s)	31.5	31.5	31.5	85.0	85.0	102.0	85.0	85.0	85.0	125.0
No. of IPs	12	12	13	15	15	15	15	11	8	5
Resolution (Å)	120 - 10	60 - 8	60 - 7	40 - 8	30 - 8	30 - 8	30 - 8	30 - 8	30 - 8	30 - 8
Completeness	0.904	0.901	0.828	0.863	0.870	0.837	0.600	0.667	0.547	0.566
Multiplicity	3.26	3.30	3.55	2.89	3.05	2.90	2.60	2.75	2.60	2.80
Rmerge	0.113	0.103	0.116	0.091	0.068	0.070	0.063	0.077	0.078	0.065

TCNPT: potassium tetracyanoplatinate(II) trihydrate, DCNAU: gold(I) potassium cyanide, TIOHG: Mercury(II) potassium iodide, COMPA: 2,6-diiodo-4-(2,2-dicyanovinyl)phenol, HMOCL: Mo_6Cl_{14} , TAMM: tetrakis(acetoxymercuri)methane.

1) Completeness = (No. of unique reflection with $F > 2\sigma_F$) / (No. of total possible reflection).
2) Multiplicity = (No. of observed reflection) / (No. of unique reflection).

3)$R_{merge} = \Sigma_h\Sigma_i \ |I_{hi} - \langle I_h \rangle| / \Sigma_h\Sigma_i \langle I_h \rangle$.

Table 3.3.V Isomorphous Differences among Native Crystals not Trated with PDTA

Lot No. (pH)	Lot 1 (8.0)	Lot 4 (8.0)	Lot 5 (8.0)	Lot 4 (7.2)	Lot 6 (7.2)
Lot 1 (8.0)	—	0.070	0.119	0.099	0.148
Lot 4 (8.0)	2739	—	0.118	0.086	0.133
Lot 5 (8.0)	4791	2528	—	0.111	0.144
Lot 4 (7.2)	5763	2729	4961	—	0.126
Lot 6 (7.2)	5772	2718	4988	5932	—

Upper-right: isomorphous difference = $\Sigma_{\text{crystal}}\Sigma_h |F_{h\,\text{crystal}} - \langle F_h \rangle| / \Sigma_{\text{crystal}}\Sigma_h \langle F_h \rangle$,
Lower-left: No. of common reflections.

Table 3.3.VI Isomorphous Differences among Crystals Trated with PDTA

Lot No.	Lot 1	Lot 2	Lot 3	Lot 4
Lot 1	—	0.143	0.163	0.139
Lot 2	3169	—	0.076	0.070
Lot 3	6015	3215	—	0.063
Lot 4	4653	2589	4527	—

Upper-right: isomorphous difference = $\Sigma_{\text{crystal}}\Sigma_h |F_{h\,\text{crystal}} - \langle F_h \rangle|$
$/\Sigma_{\text{crystal}}\Sigma_h \langle F_h \rangle$, Lower-left: No. of commo reflections.

Table 3.3.VII Isomorphous Differences between Derivatives and Corresponding Native

	data set 1 (Lot 1)	data set 2 (Lot 4)		
Derivative	PDTA	PDTA	TAMM	HMOCL
Resolution (Å)	30 - 8	30 - 8	30 - 8	30 - 8
R_{deriv}	0.227	0.122	0.117	0.116

$R_{\text{deriv}} = \Sigma_h |F_h(\text{derivative}) - F_h(\text{native})| / \Sigma_h \langle F_h(\text{native}) \rangle$.

Table 3.3.VIII Isomorphous Differences of PDTA Treated Derivatives

Derivative	data set 1 (Lot 2) TCNPT	data set 2 (Lot 3) DCNAU	TCNPT	TIOHG	COMPA	data set 3 (Lot 4) TAMM	HMOCL
Resolution (Å)	60 - 10	60 - 10	30 - 8	30 - 8	30 - 8	30 - 8	30 - 8
R_{deriv}	0.071	0.062	0.057	0.060	0.149	0.132	0.054

$R_{deriv} = \Sigma_h |F_h(\text{derivative}) - F_h(\text{native})| / \Sigma_h \langle F_h(\text{native})\rangle$.

Table 3.3.IX *X* and *Y* Coordinates of Heavy-atom Sites of TAMM and HMOCL Derivative Deduced from Difference Patterson Map

TAMM	$z = 1/6$	$z = 1/3$	$z = 1/2$	mean
Site 1	(0.37, 0.08)	(0.35, 0.07)	(0.36, 0.06)	(0.360, 0.070)
Site 2	(0.50, 0.08)	(0.49, 0.07)	(0.50, 0.06)	(0.497, 0.070)
Site 3	(0.47, 0.35)	(0.46, 0.33)	(0.44, 0.31)	(0.457, 0.330)
HMOCL	$z = 1/6$	$z = 1/3$	$z = 1/2$	mean
Site 1	(0.48, 0.12)	(0.46, 0.10)	(0.46, 0.08)	(0.467, 0.100)
Site 2	(0.23, 0.20)	(0.21, 0.22)	(0.23, 0.19)	(0.223, 0.203)
Site 3	(0.31, 0.31)	(0.29, 0.29)	(0.29, 0.31)	(0.297, 0.303)
Site 4	(0.46, 0.33)	(0.43, 0.31)	(0.42, 0.31)	(0.437, 0.317)
Site 5	(0.27, 0.12)	(0.27, 0.16)	(0.23, 0.10)	(0.257, 0.127)

The columns of $z = 1/6$, $z = 1/3$ and $z = 1/2$ showed the x and y coordinates of the heavy-atom sites deduced from the peaks on each Harker section in the difference Patterson map of each derivatives. The column of mean showed the mean coordinates of the columns of $z = 1/6$, $z = 1/3$ and $z = 1/2$.

Table 3.3.X Z Coordinate of Peaks Located at the End of Cross-vector

HMOCL	(x, y) of cross-vector	z coordinates of peaks
Site 1 — Site 2	(-0.244, 0.103) :	0.05, 0.10, 0.19, 0.27, 0.42
Site 1 — Site 3	(-0.170, 0.203) :	0.10, 0.16, 0.21
Site 1 — Site 4	(-0.030, 0.217) :	0.08, 0.12, 0.24, 0.36
Site 1 — Site 5	(-0.210, 0.027) :	0.02, 0.08, 0.29, 0.37, 0.47
Site 2 — Site 3	(0.074, 0.100) :	0.01, 0.05, 0.11, 0.21, 0.27
Site 2 — Site 4	(0.214, 0.114) :	0.02, 0.13, 0.18, 0.29, 0.31, 0.47
Site 2 — Site 5	(0.034, -0.076) :	0.05, 0.22, 0.36, 0.43
Site 3 — Site 4	(0.140, 0.014) :	0.08
Site 3 — Site 5	(-0.040, -0.176) :	0.08, 0.13, 0.28, 0.42, 0.47
Site 4 — Site 5	(-0.180, -0.190) :	0.08, 0.18, 0.24, 0.37, 0.48
TAMM	(x, y) of cross-vector	z coordinates of peaks
Site 1 —S ite 2	(0.137, 0.000) :	0.08, 0.12, 0.22, 0.30, 0.41
Site 1 — Site 3	(0.097, 0.260) :	0.02, 0.08, 0.18, 0.20, 0.27, 0.37
Site 2 — Site 3	(-0.040, 0.260) :	0.02, 0.13, 0.31, 0.42, 0.47

The (x, y) of cross-vectors of each row were obtained from the coordinates listed in Table 3.3.IX.

Table 3.3.XI Results of Single Isomorphous Replacement with One Site

	TAMM			HMOCL				
No. of reflection (centric / Acentric)	5318 (45 / 5273)			5474 (45 / 5429)				
	Site 1	Site 2	Site 3	Site 1	Site 2	Site 3	Site 4	Site 5
x	0.359	0.497	0.448	0.465	0.222	0.297	0.438	0.256
y	0.068	0.070	0.350	0.100	0.203	0.304	0.318	0.130
Occupancy	2.291	2.428	1.970	3.989	4.350	4.302	4.111	4.349
R_{Cullis}	0.768	0.656	0.655	0.760	0.592	0.634	0.657	0.664
R_{Kraut}	0.173	0.175	0.169	0.163	0.167	0.169	0.166	0.171
No. of reflections (Fom > 0.2)	2323	2575	1782	1931	2318	2159	2158	2417
Mean Fom	0.268	0.291	0.272	0.263	0.274	0.270	0.268	0.278
Phasing power	1.32	1.42	1.22	1.29	1.37	1.35	1.34	1.37

$R_{\mathrm{Cullis}} = \Sigma_h \, ||F_{\mathrm{PH}} - F_{\mathrm{P}}| - |F_{\mathrm{H\,calc}}|| / \Sigma_h \, ||F_{\mathrm{PH}}| - |F_{\mathrm{P}}||$, where summed over centric reflection,

$R_{\mathrm{Kraut}} = \Sigma_h \, ||F_{\mathrm{PH}} - F_{\mathrm{P}}| - |F_{\mathrm{H\,calc}}|| / \Sigma_h \, ||F_{\mathrm{PH}}| - |F_{\mathrm{P}}||$, where summed over acentric reflection,

Fom: figure of merit $\cos(\Delta\alpha_{\mathbf{h}})$, where $\Delta\alpha_{\mathbf{h}}$ is the error in phase angle for reflection **h**,

phasing power is defined as ⟨isomorphous difference⟩/⟨lack of closure⟩.

Table 3.3.XII Z Coordinates of Peaks of Heavy-atom Sites in Difference Fourier Map of TAMM Derivative

Site	(x, y)	z of peaks
In the map phased with Site 1		
Site 2	(0.497, 0.070)	: 0.03, 0.25, 0.65, 0.88
Site 3	(0.457, 0.330)	: 0.28, 0.80
In the map phased with Site 2		
Site 1	(0.360, 0.070)	: 0.12, 0.70
Site 3	(0.457, 0.330)	: 0.51
In the map phased with Site 3		
Site 1	(0.360, 0.070)	: 0.16, 0.21, 0.46, 0.61, 0.75
Site 2	(0.497, 0.070)	: 0.19, 0.35, 0.48, 0.65, 0.70, 0.91

Table 3.3.XIII Results of Single Isomorphous Replacement with Site 1 and 2 of TAMM derivative

	TAMM	
No. of reflection (centric / Acentric)	5318 (45 / 5273)	
	Site 1	Site 2
x	0.357	0.497
y	0.068	0.069
z	0.000[1]	0.880
Occupancy	1.278	2.031
R_{Cullis}	0.700	
R_{Kraut}	0.169	
No. of reflections (Fom > 0.2)	2678	
Mean Fom	0.33	
Phasing power	1.45	

1) The z coordinate of Site 1was fixed to 0.0 in refinement cycle.

$R_{\mathrm{Cullis}} = \Sigma_h \, ||F_{\mathrm{PH}} - F_{\mathrm{P}}| - |F_{\mathrm{H\ calc}}||/\Sigma_h \, ||F_{\mathrm{PH}}| - |F_{\mathrm{P}}||$, where summed over centric reflection,

$R_{\mathrm{Kraut}} = \Sigma_h ||F_{\mathrm{PH}} - F_{\mathrm{P}}| - |F_{\mathrm{Hcalc}}||/\Sigma_h ||F_{\mathrm{PH}}| - |F_{\mathrm{P}}||$, where summed over acentric reflection,

Fom: figure of merit $\cos(\Delta\alpha_{\mathbf{h}})$, where $\Delta\alpha_{\mathbf{h}}$ is the error in phase angle for reflection **h**, phasing power is defined as ⟨isomorphous difference⟩/⟨lack of closure⟩.

Table 3.3.XIV The Results of Multiple Isomorphous Replacement

	TAMM		HMOCL
No. of reflection (centric / Acentric)	5318 (45 / 5273)		5474 (45 / 5429)
	Site 1	Site 2	Site 5
x	0.358	0.497	0.257
y	0.068	0.069	0.134
z	0.000[1]	0.881	0.210
Occupancy	1.459	2.149	3.695
R_{Cullis}	0.719		0.693
R_{Kraut}	0.166		0.164
No. of reflections (Fom > 0.3)	3443		3456
Mean Fom	0.332		0.271
Overall mean Fom	0.411 / 6074 refs.		
Phasing power	0.332		0.271

1) The z coordinate of Site 1 of TAMM derivative was fixed to 0.000 in refinement cycle.

$R_{\mathrm{Cullis}} = \Sigma_h \, ||F_{\mathrm{PH}} - F_{\mathrm{P}}| - |F_{\mathrm{H\,calc}}|| / \Sigma_h \, ||F_{\mathrm{PH}}| - |F_{\mathrm{P}}||$, where summed over centric reflection,

$R_{\mathrm{Kraut}} = \Sigma_h \, ||F_{\mathrm{PH}} - F_{\mathrm{P}}| - |F_{\mathrm{H\,calc}}|| / \Sigma_h \, ||F_{\mathrm{PH}}| - |F_{\mathrm{P}}||$, where summed over acentric reflection,

Fom: figure of merit, $\cos(\Delta\alpha_{\mathbf{h}})$, where $\Delta\alpha_{\mathbf{h}}$ is the error in phase angle for reflection **h**, phasing power is defined as ⟨isomorphous difference⟩/⟨lack of closure⟩.

Table 3.3.XV The Refined Heavy-atom Parameters and Statistical Data of TAMM and HMOCL

	TAMM			HMOCL		
No. of reflection (centric / Acentric)	5318 (45 / 5273)			5474 (45 / 5429)		
	Site 1	Site 2	Site 3	Site 2	Site 4	Site 5
x	0.359	0.495	0.457	0.222	0.430	0.258
y	0.063	0.066	0.351	0.206	0.321	0.135
z	0.000[1]	0.881	0.199	0.189	0.581	0.211
Occupancy	1.284	2.093	0.815	1.907	1.336	3.261
R_{Cullis}		0.680			0.709	
R_{Kraut}		0.163			0.161	
No. of reflections (Fom > 0.3)		3542			3576	
Mean Fom		0.332			0.298	
Overall mean Fom			0.429 / 6074 refs.			
Phasing power		1.69			1.44	

1) The z coodinate of Site 1 of TAMM derivative was fixed to 0.000 in refinement cycle.

$R_{\mathrm{Cullis}} = \Sigma_h \, ||F_{\mathrm{PH}} - F_{\mathrm{P}}| - |F_{\mathrm{H\,calc}}|| / \Sigma_h \, ||F_{\mathrm{PH}}| - |F_{\mathrm{P}}||$, where summed over centric reflection, $R_{\mathrm{Kraut}} = \Sigma_h \, ||F_{\mathrm{PH}} - F_{\mathrm{P}}| - |F_{\mathrm{H\,calc}}|| / \Sigma_h \, ||F_{\mathrm{PH}}| - |F_{\mathrm{P}}||$, where summed over acentric reflection, Fom: figure of merit, $\cos(\Delta\alpha_{\mathbf{h}})$, where $\Delta\alpha_{\mathbf{h}}$ is the error in phase angle for reflection **h**, phasing power is defined as ⟨isomorphous difference⟩/⟨lack of closure⟩.

Table.3.3.XVI Results of Non-crystallographic Symmetry Averaging Refinement Cycles

No.	*R*-factor	Correlation[1] coefficient	Mean Fom[2]
solvent flattening path			
1	0.454	0.823	0.657
2	0.363	0.906	0.793
3	0.323	0.928	0.860
4	0.302	0.937	0.898
5	0.291	0.941	0.921
6	0.283	0.944	0.936
7	0.277	0.946	0.947
8	0.273	0.948	0.955
Correlation coefficient around NCS two-fold axis 0.160			
NCSA path1			
9	0.370	0.902	0.726
10	0.372	0.904	0.721
11	0.368	0.908	0.723
12	0.363	0.911	0.725
13	0.359	0.914	0.727
14	0.355	0.916	0.730
15	0.353	0.917	0.731
16	0.350	0.918	0.733
17	0.349	0.919	0.733
18	0.347	0.920	0.735
19	0.345	0.921	0.736
20	0.344	0.922	0.737
21	0.342	0.922	0.738
22	0.341	0.923	0.738
23	0.340	0.923	0.739
24	0.339	0.924	0.740
Correlation coefficient around NCS two-fold axis 0.679			

No.	*R*-factor	Correlation[1] coefficient	Mean Fom[2]
NCSA path2			
25	0.365	0.915	0.711
26	0.354	0.919	0.717
27	0.347	0.923	0.723
28	0.342	0.925	0.728
29	0.338	0.927	0.732
30	0.335	0.928	0.734
31	.333	0.929	0.736
32	0.331	0.930	0.738
33	0.330	0.930	0.739
34	0.329	0.931	0.740
35	0.328	0.931	0.741
36	0.327	0.932	0.742
37	0.326	0.932	0.742
38	0.325	0.932	0.743
39	0.324	0.933	0.744
40	0.323	0.933	0.745
Correlation coefficient around NCS two-fold axis 0.688			
NCSA path3			
41	0.340	0.927	0.730
42	0.337	0.929	0.731
43	0.335	0.930	0.733
44	0.332	0.931	0.735
45	0.331	0.932	0.736
46	0.329	0.932	0.737
47	0.328	0.932	0.739
48	0.327	0.933	0.739
49	0.326	0.933	0.740
50	0.325	0.934	0.741
51	0.324	0.934	0.742
52	0.324	0.934	0.743
53	0.323	0.934	0.743
54	0.323	0.935	0.743
55	0.322	0.935	0.744
56	0.322	0.935	0.744
Correlation coefficient around NCS two-fold axis 0.708			

1) Correlation coefficient between observed structure amplitudes and calculated ones from modified electron density map.

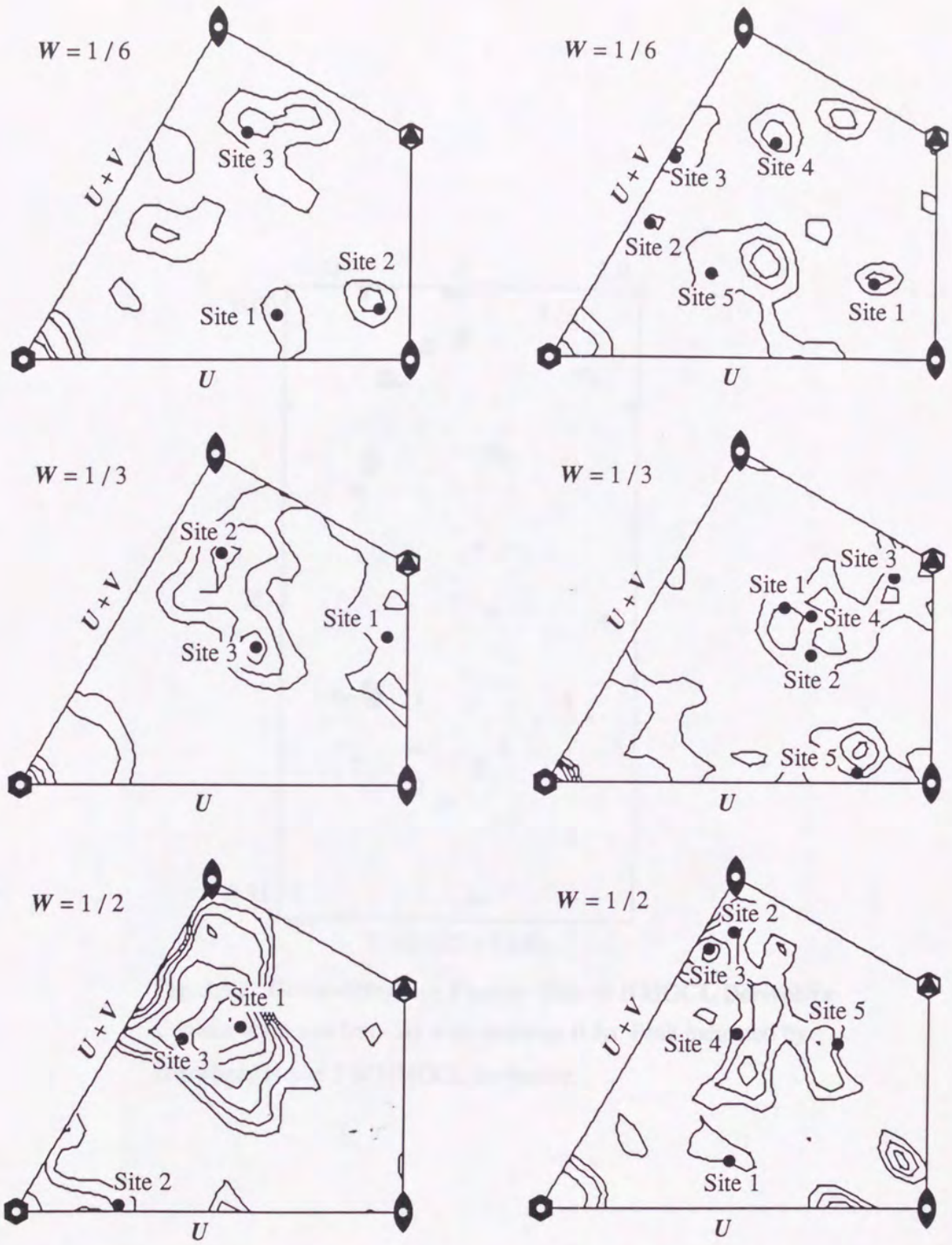

(a) TAMM

(b) HMOCL

Fig. 3.3.1. Three Harker Sections of Difference Patterson Map of TAMM and HMOCL derivatives

These maps were contoured from 1s with stepwise by 1s. The black circles represent positions corresponded to the heavy-atom site listed in Table 3.3.IX.

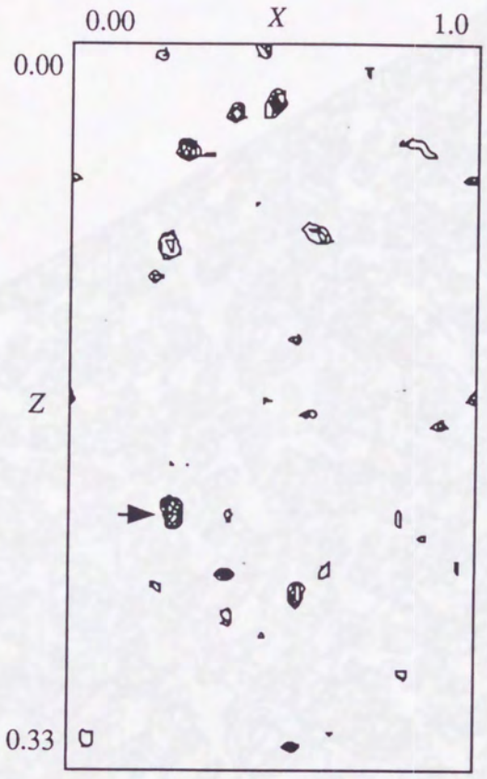

Y = 0.125 – 0.138

Fig. 3.3.2. Cross-difference Fourier Map of HMOCL Derivative
Contour level was from 2σ with stepwise 0.5σ. Peak indicated by arrowhead is Site 5 of HMOCL derivative.

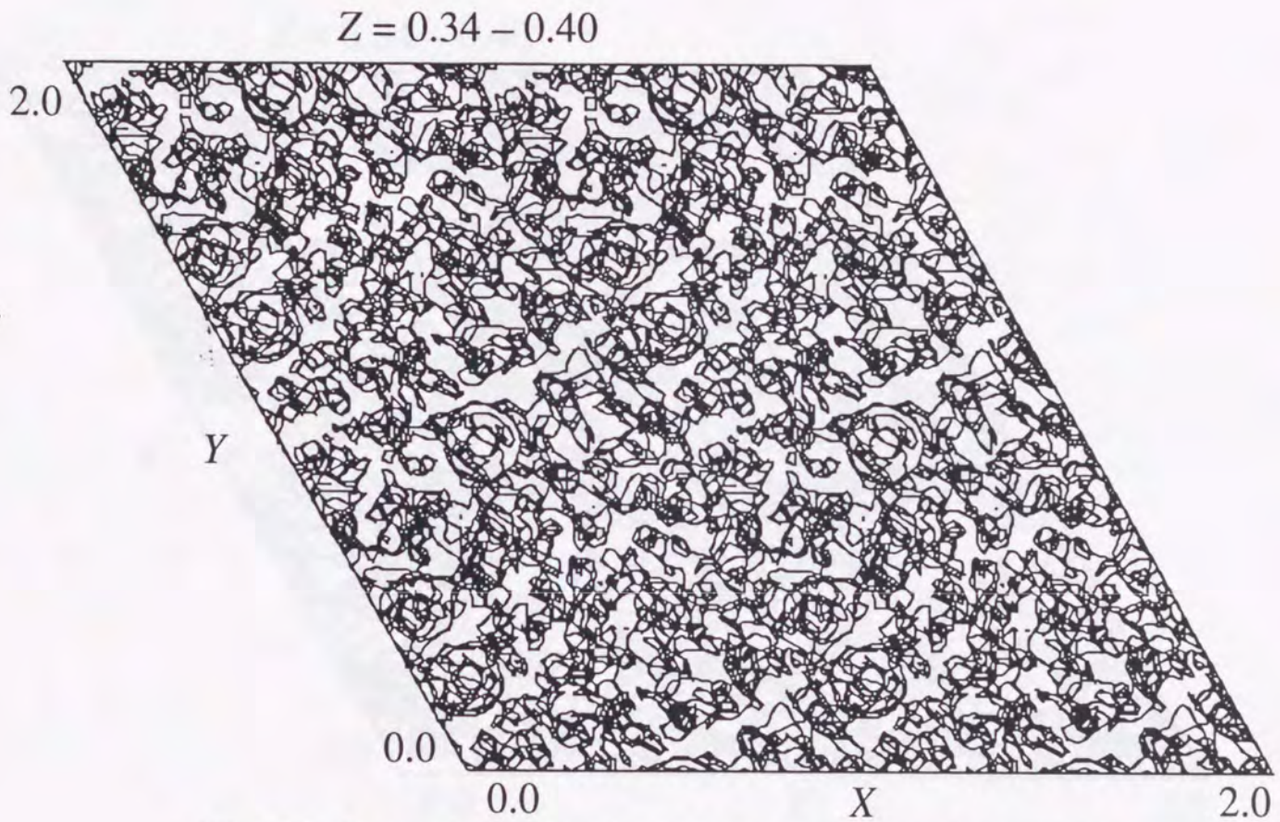

Fig. 3.3.3. Electron Density Map from Multiple Isomorphous Replacement

This map has sections from $Y = 0.34$ to 0.40. Contour levels are 1σ and 2σ.

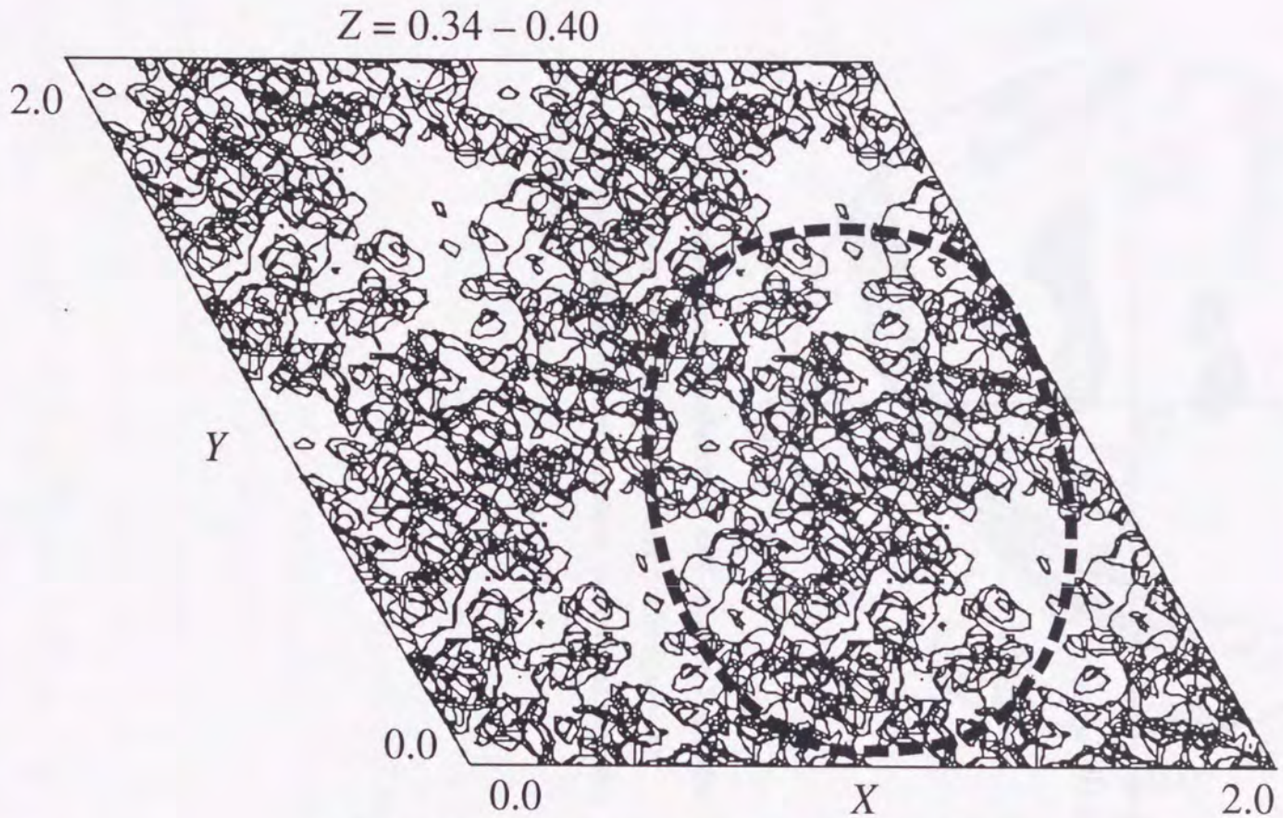

Fig. 3.3.4. Electron Density Map After Solvent Flattening

This map has sections from $Y = 0.34$ to 0.40. Contour levels are 1σ and 2σ.
Region surrounded by dashed line indicates the molecular boundary containing whole dimer.

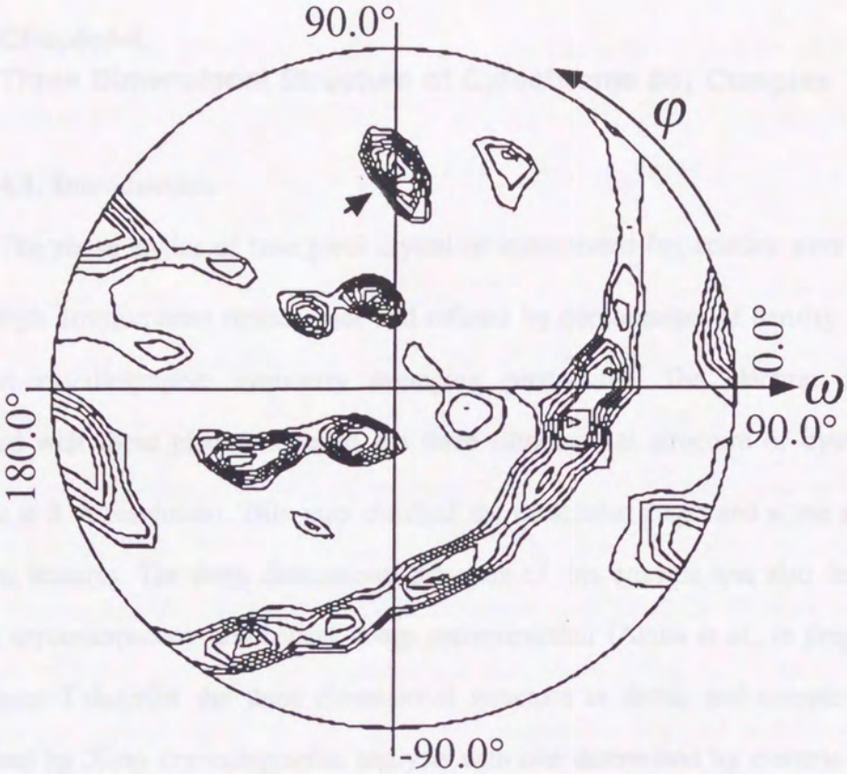

Fig. 3.3.5. Result of the Calculation of Self-rotation Function

This κ = 180 has ω = 0° or 90° at the center of circle, w = 90° around the edge, and j as marked periphery. Arrowhead indicates the highest peak.

Chapter-4.
Three Dimensional Structure of Cytochrome bc_1 Complex

4.1. Introduction

The phase angles of hexagonal crystal of cytochrome bc_1 comlex were obtained by the multiple isomorphous replacement and refined by combination of density modification and non-crystallographic symmetry averaging procedures. The electron density map calculated with these phases revealed the three dimensional structure of cytochrome bc_1 complex at 8 Å resolution. This map clarified the molecular shape and some characteristic structural features. The three dimensional structure of this enzyme was also determined by electron cryomicroscopy and helical image reconstruction (Akiba *et al.*, in preparation). In this chapter I describe the three dimensional structure in detail, and compare the model determined by X-ray crystallographic analysis with one determined by electron microscopic analysis.

4.2. Structure of the bc_1 complex determined by X-ray analysis and comparison with model determined by electron microscopic analysis

Shape of molecule — Views of the cyctochrome bc_1 comlex dimer determined by X-ray crystallographic analysis (X-ray model) are shown in Fig. 4.1. The size of the dimer was about 150 Å along and 100 x 130 Å perpendicular to the two-fold axis. This size was consistent with the model determined by the electron microscopic analysis (EM model). It is reported about the structure of cytochrome bc_1 complex that this enzyme elongates across the membrane projecting ~70 Å into the matrix side of mitochondoria and ~30 Å into the intermembrane space (IMS) side (Leonard *et al.*, 1981; Karlsson *et al.*, 1983; Akiba *et al.*, in preparation). The transmembrane region of X-ray model was assigned as illustrated in

Fig.4.1. On the basis of electron microscopic results this enzyme may be divided into three regions: the intermembrane space (IMS) domain, the matirx domain and the transmembrane region connecting these domains. X-ray and EM models of each domain were compared. Fig. 4.2 shows the X-ray model with contour stacks cut in various planes to display from the intermembrane space.

Structure of intermembrane space domain — The IMS domains of both X-ray and EM models are composed of three portion: two bulbs (Bb1, Bb2 in Fig. 4.2.*a*) and a disk (Dk in Fig. 4.2.*a*). Each of the two bulbs is apart about 20 Å from two-fold axis. Two bulbs are rooted to the disk. The mass of disk region of X-ray model is smaller than that of EM model. Though the disk mass of EM model is spread on the surface of membrane and partly buried in the surface layer of the membrane, that of X-ray model seems to be composed of five columns and not buried into the surface of membrane. The EM model has flat lobular structures spreading along the membrane at the depth of its hydrophilic layer. The X-ray model also has similar structure, however they are not flat but like arm (Am in Fig. 4.2.*b*).

Structure of transmembrane region — The transmembrane region consists of a flat column (Tm in Fig. 4.2.*c*) vertically across the lipid bilayer. The transmembrane region of X-ray model is apart about 10 Å from the two-fold axis. In EM model transmembrane is composed of two separated segments: the large one having complex shape and the small one separated ~10 Å from the large segment. These segments seem to fuse each other in the X-ray model. The transmembrane region runs through the membrane from the disk of IMS domain to 'neck' part of matrix domain (Nk in Fig. 4.2.*d*) so that the whole dimer twists clockwise about 60° around its two-fold axis in this region.

Structure of matrix domain — The neck part of matrix domain (Nk in Fig. 4.2.*d*) is apart about 5 Å from two-fold axis, then this region is considered the intra-dimer contact region. This part in the EM model is more separated each other by about 25 Å and more complicated structure spreading along the surface of lipid bilayer of matrix side. There are not these spreading structures in X-ray model. The whole dimer structure of matrix domain

of X-ray model is like shell. Inside the matrix domains the dimer is empty in oval shape (Ep in Fig. 4.2.*e*), which has a long diameter of about 45 Å and a short diameter of about 25 Å and opens off to the extra-molecule (Mt1 and Mt2 in Fig. 4.2.*e*). In the matrix domain of EM model, this empty region is separated into two cavities each of which has a diameter of about 25 Å and has only one aperture at the corresponding position of Mt2 of the X-ray model. In the X-ray model the center of oval empty region corresponds to the heavy -atom binding site of Site 2 of TAMM. The electron density map calculated with MIR phases has a large ripple around this site, therefore it is likely that the two cavities seem to be appeared as one oval empty region. The matrix domain carries two bulges (Bg1 and Bg2 in Fig. 4.2.*e*). These bulges are in contact with neighboring molecules in crystal lattice (Fig. 4.3). Same structures as present in the EM model and they also connect to neighboring molecules in tublular crystals. Akiba *et al.* proposed that these regions were zinc cation binding site by following reasons: (1) molecules contact to neighboring one only at these positions in tubular crystals, (2) zinc cation is essential to forming the tubular crystals, (3) these positions were assigned to core I and/or II subunit and zinc cation was bound to those subunits (Lorusso *et al.*, 1991). The X-ray model would support their supposition.

The X-ray model is intrinsically similar to the model determined by electrrn microscopic analysis (Akiba *et al.*, in preparation), however, there are some differences around the surface of lipid bilayer as described above. Hydrophilic head group of phospholipids surrounding the transmembrane regions of membrane protein generally give high densities in the electron microscopic map. Therefore, the differences between X-ray and EM model might be arised because the densities of the hydrophilic surface of lipid bilayer were interpreted as those of the protein in the EM model.

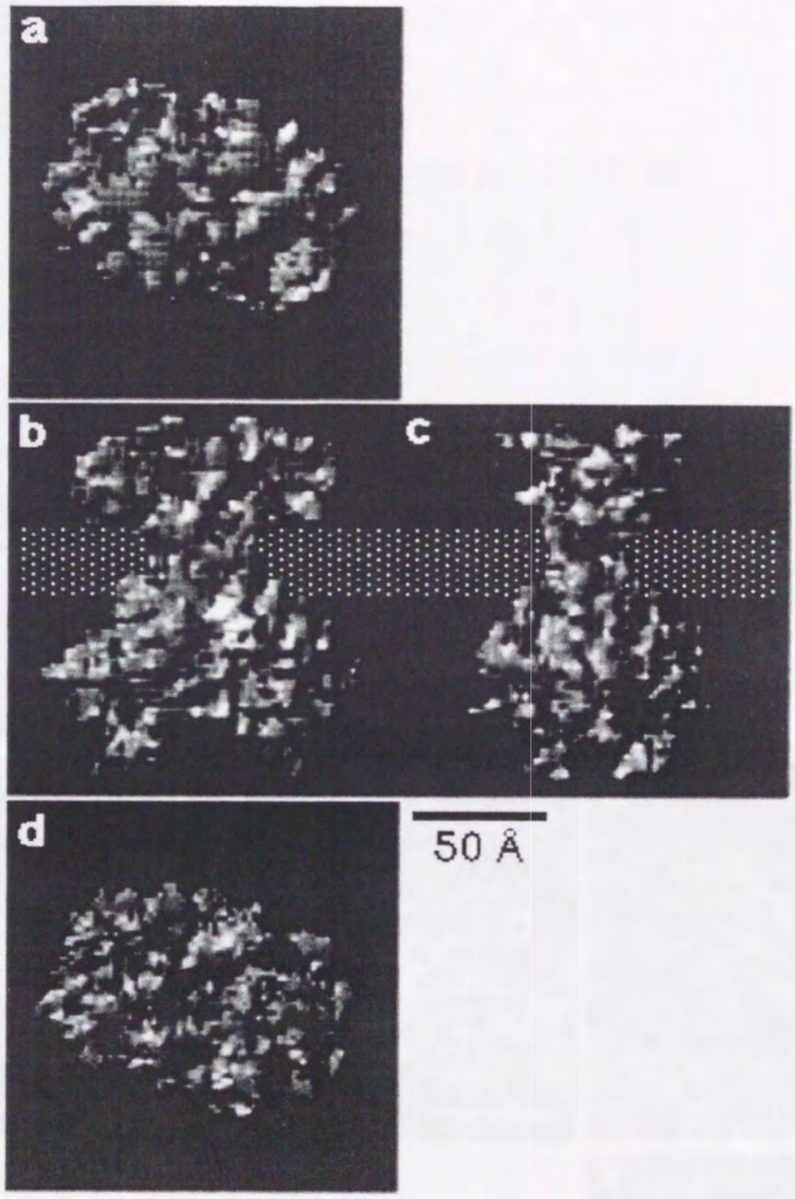

Fig. 4. 1 Surface Models of Cytochrome a_3 Complex

a) View of the figure b) from intermembrane space (top of this paper).

d) View of the figure b) from matirx side (bottom of this paper).

c) This model was rotated the b) around their dimeric two-fold axis.

Gray regions of b) and c) indicate lipid bilayer.

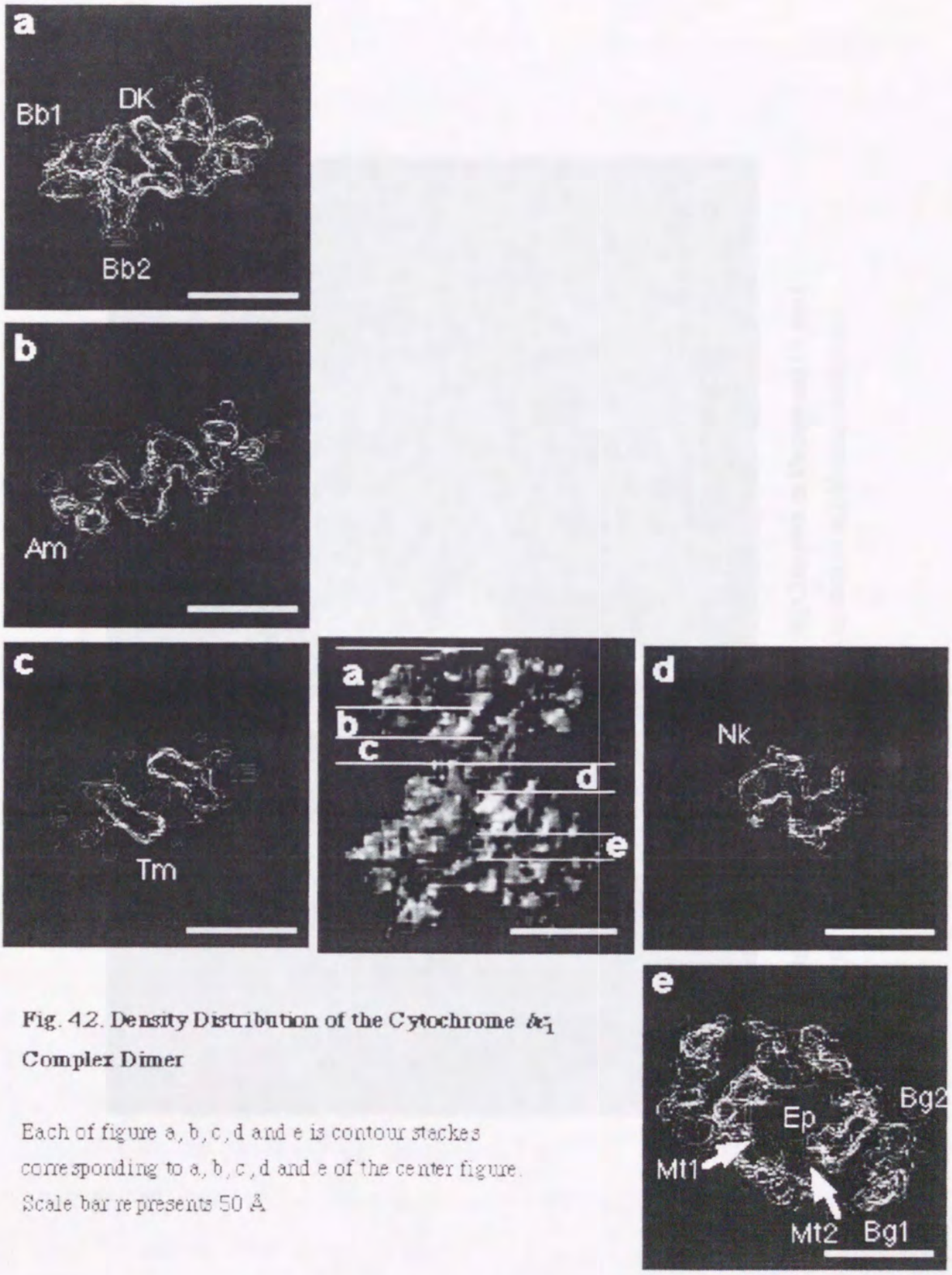

Fig. 4.2. Density Distribution of the Cytochrome bc_1 Complex Dimer

Each of figure a, b, c, d and e is contour stackes corresponding to a, b, c, d and e of the center figure. Scale bar represents 50 Å

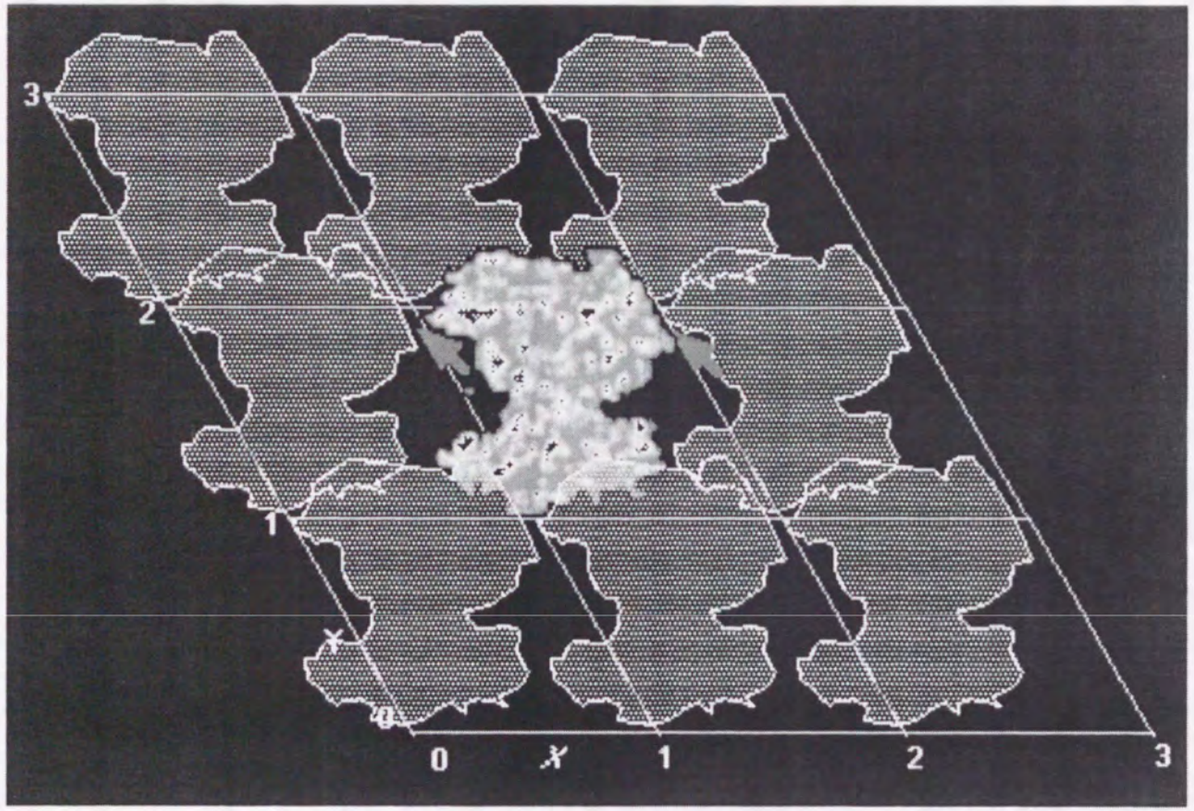

Fig. 4. 3. Packing of Cytochrome bc_1 Complex in Hexagonal Crystal

Green arrow indicates the region to contact to neighboring molecules.

Conclusion

Cytochrome bc_1 complex from bovine heart mitochondoria was crystallized in the hexagonal under potassium phosphate buffer. This crystal form had problems in reproducibility and quality. As a result of the survey of divalent metal cation as additive, the addition of $ZnCl_2$ to the crystallization solution was effective for the improvement of the reproducibility of crystallization and the quality of the crystals. The crystals grown in the presence of $ZnCl_2$ gave better diffraction intensities than those grown in its absence. Using crystals grown in the presence of $ZnCl_2$ preparation of heavy-atom derivative crystals were attempted. Two derivatives, tetrakis(acetoxymercuri)methane (TAMM) and Mo_6Cl_{14} (HMOCL), were obtained. The diffraction intensities of the native and these two derivative crystals were collected with sufficient quality for X-ray crystallographic analysis to 8 Å resolution. Phase angles were calculated by the multiple isomorphous replacement method using these derivative crystals, and refined by the solvent flattening and the non-crystallographic symmetry averaging. The electron density map calculated with the resultant phases clarified the three dimensional structure of this enzyme at 8 Å resolution. The three dimensional structure of this enzyme determined by the X-ray crystallography has a size of about 150 x 130 x 100 Å and revealed some characteristic structural features: two bulbs of the intermembrane space domain, narrow transmembrane region and large hollow structure of matrix domain. These structural features were also found in the three dimensional structure determined by the electron microscopic analysis.

At present the resolution of the structure of cytochrome bc_1 complex is limited to 8 Å resolutio. It wase repored that recrystallization was useful for improving the quality of the crystals for this enzyme (Matunaga, 1995; Kubata, in preparation). By using the recrystallized crystals data collection of higher resolution data and have more detailed structure of this enzyme may be expected.

Acknowledgments

The present work has been carried out under the direction of Professor Keiichi Fukuyama of Faculty of Science, Osaka University. I would like to thank him for his incessant guidance and encouragement throughout this work. I am deeply indebted to Professor Shinya Yoshikawa, Himeji Institute of Technology, for his invaluable advice and discussion. I am also grateful to Dr. Kyoko Itoh, Himeji Institute of Technology, for her technical advice and helpful suggestion.

I am deeply indebted to Professor Tomitake Tsukihara, Osaka University, for incessant encouragement and helpful advice to X-ray crystallography. I am also deeply grateful to Professor Noriyoshi Sakabe, Dr. Atsushi Nakagawa, Dr. Nobuhisa Watanabe and Dr. Shinji Ikemizu of Photon Facttory, National Laboratory for High Energy Physics for their kind help with the data collection.

I like to thank Mr. Tsurusawa, Municipal Abattoir, Kobe, for kind donation of fresh bovine heart.

I express my thanks to all members in Fukuyama's, Yoshikawa's and Tsukihara's laboratories for their kind assistances and encouragement.

Finally, I thank my parents and my sister for thier incessant understanding and encouragement.

Reference

Anderson, S., de Buruijn, M. H. L., Coulson, A. R., Eperon, I. C., Sanger, F. & Young I. G. (1982). *J. Mol. Biol.* **159**, 638-717.

Bell, R. L., Sweetland, J., Ludwig, B. & Capaldi, R. A. (1979). *Proc. Nat. Acad. Sci., U.S.A.* **76**, 741-745.

Berry, E. A., Huang, L., Earnest, N., T. & Jap, B. K. (1992). *J. Mol. Biol.*, **224**, 1161-1166.

Borchart, U., Machleit, W., Schägger, H., Link, T. A. & von Jagow, G. (1985). *FEBS Lett.*, **191**, 125-130.

Borchart, U., Machleidt, W., Schägger, H., Link, T. A. & von Jagow, G. (1986). *FEBS Lett.*, **200**, 81-86.

Bricogne, G. (1976). *Acta Cryst.*, **A32**, 832-.

CCP4, (1986). The Co-operative Computing Project in Crystallography SERC Daresbury Laboratory, Warrington, UK.

Crofts, A. R., Meinhardt, S. W., Jones, K. R. & Snozzi, M. (1983). *Biochim. Biophys. Acta*, **723**, 202-218.

Crofts, A., Robinson, H., Andrew, K., van Doren, S. & Berry, E. (1988). In Cytochrome Systems (Papa, S. et al., eds), pp. 617-624, Plenum Press, NY.

Deisenhofer, J. & Michel, H. (1989). *EMBO J.*, **8**, 2149-2170.

De Vries, S., Albracht, S. P. J., Berden, J. A. & Slater, E. C. (1982). *Biochem. Biophys. Acta.* **681**, 41-53.

De Vries, S. (1986). *J. Bioenerg. Biomemb.*, **18**, 195-224.

D'souza, M. P. & Wilson, D. F. (1982). *J. Biol. Chem.* **257**, 11760-11766.

Esposti, M. D. & Lenaz, G. (1982). *FEBS Letters* **142**, 45-53.

Furey, W. and Swaminathan, S. (1990). American Crystallographic Association Mtg. Abstr. Ser. 2 18, 73-.

Gencic, S., Schögger, H. & von Jagow, G. (1991). *Eur. J. Biochem.*, **199**, 123-131.

Gonzalez-Halphen, D., Lindorfer, M. A. & Capaldi, R. A. (1988). *Biochemistry* **27**, 7021-7031.

Green, D.W., Ingram, V.M. & Perutz, M.F. (1954). *Proc. Roy. Soc.*, **A225**, 287-.

Gros, P., Groendijk, H., Drenth, J. & Hol, W. G. J. (1988). *J. Crystal Growth* **90**, 193-200.

Hatefi, Y., Haavik, A. G. & Griffiths, D. E. (1962). *J. Biol. Chem.*, **237**, 1681-1685.

Hatefi, Y. & Yagi, T. (1982). *Biochemistry* **21**, 6614-6618.

Hatefi, Y. (1985). *Ann. Rev. Biochem*, **54**, 1015-1069.

Hauska, G., Hurt, E., Gabellini, N. & Lockau, W. (1983). *Biochim. Biophys. Acta* **726**, 97-133.

Higashi, T. (1989). *J. Appl. Cryst.*, **22**, 9-18.

Karlsson, B., Hovmo\eller, S., Weiss, H. & Leonard, K. (1983). *J. Molec. Biol.* **165**, 287-302.

Kauten, R., Tsai, A.-L. & Palmer, G. (1987). *J. Biol. Chem.* **262**, 8658-8667.

Kawamoto, M. (1993). Masteral thesis, Osaka Univ. Osaka, Japan.

Kubota, T., Kawamoto, M., Fukuyama, K., Shinzawa-Ito, K., Yoshikawa, S. & Matsubara, H. (1991). *J. Mol. Biol.*, **221**, 379-382.

Kubota, T., Yoshikawa, S. & Matsubara, H. (1992). *J. Biochem.*, **111**, 91-98.

Kubota, T. (1993). Doctorral thesis, Osaka Univ. Osaka, Japan.

Kühlbrandt, W. (1988). *Quarterly Rev. Biophys.*, **21**, 429-477.

Leonard, K., Wingfield, P., Arad, T. & Weiss, H. (1981). *J. Molec. Biol.* **149**, 259-274.

Li, Y., Leonard, K. & Weiss, H. (1981a). *FEBS Letters* **116**, 199-205.

Li, Y., DeVries, S., Leonard, K. & Weiss, H. (1981b). *FEBS Letters* **135**, 277-280.

Link, T. A., Schägger, H. & von Jagow, G. (1986). *FEBS Letters* **204**, 9-15.

Lorusso, M., Cocco, T., Sardanelli, A. M., Minuto, M., Bonomi, F. & Papa, S. (1991). *Eur. J. Biochem.* **197**, 555-561.

Matthews, B. W. (1968). *J. Mol. Biol.*, **33**, 491-497.

Mitchell, P. (1976). *J. Theor. Biol.* **62**, 327-367.

Miyamoto, K. (1994). *Chemistry Letters*, 1971-1974.

Muatov, A. & Robinson, N. C. (1994). *Biochemistry* **33**, 10561-10567.

Ozawa, T., Tanaka, M. & Shimomura, Y. (1980). *Proc. Nat. Acad. Sci., U.S.A.* **77**, 5084-5086.

Perutz, M. F. (1956). *Acta. Cryst.*, **9**, 867-.

Rieske, J. S. (1967). *Methods Enzymol.*, **10**, 239-245.

Rieske, J. S. (1971). *Arch. Biochem. Biophys.*, **145**, 179-193.

Sakabe, N. (1983). *J. Appl. Cryst.*, **16**, 542-547.

Sarraste, A. (1984). *FEBS Letters* **166**. 367-372.

Schägger, H. & von Jagow, G. (1983). *Hoppe-Seyler Z. Physiol. Chem.*, **364**, 307-311.

Schägger, H., Borchart, U., Aquila, H., Link, T. A. & von Jagow, G. (1985). *FEBS Lett.*, **190**, 89-94.

Schägger, H., Link, T. A., Engel, W. D. & von Jagow, G. (1986). *Methods Enzymol.*, **126**, 224-237.

Schägger, H., Borchart, U., Machleit, W., Link, T. A. & von Jagow, G. (1987). *FEBS Lett.*, **219**, 161-168.

Steigmann, W. (1974). Ph. D. thesis, Technical Univ. Munich.

Tokutake, N., Miyoshi, H. and Iwamura, H. (1992). *Biosci. Biotech. Biochem.* **56** (6). 919-923.

Trumpower, B. L. (1990). *Microbiol. Rev.* **54**, 101-129.

Tzagoloff, A., Yang, P. C., Wharton, D. C. & Rieske, J. S. (1965). *Biochim. Biophys. Acta*, **96**, 1-8.

Usui, S., Yu, L., harmon, J. & Yu, C.-A. (1991). *Arch. Biochem. Biophys.* **289**, 109-117.

Von Jagow, G., Ljungdahl, D. O., Graf, P., Onishi, T. & Trumpower, B. L. (1984). *J. Biol. Chem.* **259**, 6318-6326.

Wakabayashi, S., Matsubara, H., Kim, C.-H. & King, T. E. (1982a). *J. Biol. Chem.*, **257**, 9335-9344.

Wakabayashi, S., Takeda, H., Matsubara, H., Kim, C.-H. & King, T. E. (1982b). *J. Biochem.*, **91**, 2077-2085.

Wang, B.-C. (1985). *Methods Enzymol.*, **115**, 90-.

Weiss, H. & Kolb, H. J. (1979). *Eur. J. Biochem.*, **99**, 139-149.

Weiss, H. (1987). *Curr. Top. Bioenergetics* **15**, 67-90.

Weiss, M. S., Wacker, T., Weckesser, J., Welte, W. & Schulz, G. E. (1990). *FEBS Lett.*, **267**, 268-272.

Widger, W. R., Cramer, W. A., Herrmann, R. G. & Trebst, A. (1984). *Proc. Nat. Acad. Sci., U.S.A.* **81**, 674-678.

Wikström , M. & Krab, K. (1986). *J. Bioenerg. Biomembr.*, **18**, 181-193.

Yang, X. & Trumpower, B. L. (1986). *J. Biol. Chem.* **261**, 12282-12289.

Yoshikawa, S., Choc, M. G., O'Toole, M. C. & Caughey, W. S. (1977). *J. Biol. Chem.*, **252**, 5498-5508.

Yue, W.-H., Zou, Y.-P., Yu, L. & Yu, C.-A. (1991). *Biochemistry* **30**, 2303-2306.

Yu, L. & Yu, C.-A. (1993). *J. BIoenerg. Biomemb.*, **25**, 259-273.